

Published in final edited form as:

Neuron. 2009 September 10; 63(5): 657–672. doi:10.1016/j.neuron.2009.08.022.

Differences in cortical vs. subcortical GABAergic signaling: a candidate mechanism of electroclinical dissociation of neonatal seizures

J. Glykys^{1,*}, V.I. Dzhalal^{1,*}, K.V. Kuchibhotla^{1,4}, G. Feng², T. Kuner³, G. Augustine², B.J. Bacskai¹, and K.J. Staley¹

¹ Department of Neurology, Massachusetts General Hospital, Harvard Medical School, Boston, MA

² Department of Neurobiology, Duke University Medical Center, Durham, NC, and Program in Neuroscience and Behavioral Disorders, Duke-National University of Singapore Graduate Medical School, Singapore

³ Institute of Anatomy and Cell Biology, University of Heidelberg, Heidelberg, Germany

⁴ Program in Biophysics, Harvard University

Abstract

Electroclinical dissociation of neonatal seizures refers to electrographic seizure activity that is not clinically manifest. Dissociation increases after treatment with Phenobarbital, which increases the GABA_A receptor (GABA_AR) conductance. The effects of GABA_AR activation depend on the intracellular Cl⁻ concentration ([Cl⁻]_i) that is determined by the inward Cl⁻ transporter NKCC1 and the outward Cl⁻ transporter KCC2. Differential maturation of Cl⁻ transport observed in cortical vs. subcortical regions should alter the efficacy of GABA-mediated inhibition. In perinatal rat pups, most thalamic neurons maintained low [Cl⁻]_i, and were inhibited by GABA. Phenobarbital suppressed thalamic seizure activity. Most neocortical neurons maintained higher [Cl⁻]_i, and were excited by GABA_AR activation. Phenobarbital had insignificant anticonvulsant responses in the neocortex until NKCC1 was blocked. Regional differences in the ontogeny of Cl⁻ transport may thus explain why seizure activity in the cortex is not suppressed by anticonvulsants that block the transmission of seizure activity through subcortical networks.

Keywords

NKCC1; KCC2; neonatal; thalamus; neocortex; electroclinical dissociation; chloride; two-photon; imaging

Introduction

The neurotransmitter GABA, by binding to its ionotropic receptor (GABA_AR), mediates the flux of Cl⁻ and HCO₃⁻ in neurons. The opening of these receptors produces an inhibitory or excitatory response depending on the reversal potential for GABA (E_{GABA}), mediated mainly

Address correspondence to: Dr. Kevin J. Staley, Department of Neurology, Massachusetts General Hospital, 55 Fruit Street, WAC 708D, Boston, MA 02114. kstaley@partners.org.

*Co-first authors

Author contribution: JG: design, electrophysiology, two-photon imaging, analysis, writing; KK, DV: two-photon imaging and analysis; GF, TK and GA: mice generation; BJB: two-photon imaging; KJS: design, writing.

by the intracellular Cl^- concentration ($[\text{Cl}^-]_i$), and its relation to the neuron's resting membrane potential (RMP). If E_{GABA} is negative to RMP, GABA_{A} R activation will lead to an influx of Cl^- and inhibition. However, if E_{GABA} is positive to RMP, GABA_{A} R activation will mediate the efflux of Cl^- . This efflux depolarizes the membrane potential and can trigger mechanisms of neuronal excitation such as activation of voltage-gated cation channels.

Immature neurons maintain a high $[\text{Cl}^-]_i$ so that GABA_{A} R activation leads to Cl^- efflux and membrane depolarization, while mature neurons maintain a low $[\text{Cl}^-]_i$ so that GABA_{A} R activation leads to hyperpolarization (Ben-Ari et al., 2007; Kahle et al., 2008). The neuronal $[\text{Cl}^-]_i$ is set by the balance of Cl^- fluxes across the neuronal membrane. These fluxes include Cl^- movement through GABA_{A} R channels (Huguenard and Alger, 1986; Staley and Proctor, 1999; Thompson and Gahwiler, 1989), voltage gated Cl^- channels (Staley, 1994), the $\text{Cl}^-/\text{HCO}_3^-$ exchanger (Gonzalez-Islas et al., 2009), and in particular, two cation-chloride co-transporters: NKCC1, an electroneutral importer of Cl^- , and KCC2, an electroneutral extruder of Cl^- (Payne et al., 2003). NKCC1 is highly expressed in the hippocampus and neocortex at birth in rodents and humans (Dzhala et al., 2005; Plotkin et al., 1997; Wang et al., 2002). High levels of NKCC1 expression are correlated with an elevated $[\text{Cl}^-]_i$ (Brumback and Staley, 2008; Shimizu-Okabe et al., 2002). During early post-natal development, as NKCC1 expression decreases, and KCC2 expression increases. This change in transporter expression has been demonstrated to underlie the lowering of neuronal $[\text{Cl}^-]_i$ in the hippocampus (Dzhala et al., 2005; Rivera et al., 1999). However, the transition from NKCC1 to KCC2 expression does not occur synchronously throughout the whole central nervous system (Stein et al., 2004).

The ontogeny of KCC2 mRNA expression follows a caudal-rostral pattern. Spinal cord and subcortical neurons begin to express KCC2 early during embryogenesis, while KCC2 expression in cortical neurons increases after birth (Stein et al., 2004; Wang et al., 2002). These expression patterns of NKCC1 and KCC2 suggests that at birth, GABA should have a more inhibitory effect in spinal and subcortical neurons compared to cortical neurons, but there is no direct evidence for a differential effect of GABA on cortical versus subcortical structures.

We considered the possibility that the clinical manifestation of cortical seizure activity is influenced by differences in cortical vs. subcortical ontogeny of the Cl^- transporters that determine the polarity of GABA_{A} currents. Convulsions are the muscle contractions arising as a consequence of cortical electrographic seizures. However, cortical seizure activity is neither necessary (Kreindler et al., 1958) nor sufficient (Gale, 1992) for convulsive activity. For example, absence seizures involve the most of the cortex but do not cause convulsions (Hughes 2009). Convulsions can be blocked by selective inhibition of subcortical structures (Iadarola and Gale, 1982). 2-deoxyglucose, Fos, and single positron emission computed tomography studies indicate that cortical seizure activity that does not produce convulsive activity activates only the cortex, whereas seizure activity that produces convulsions also activates subcortical structures including the thalamus (White and Price, 1993; Blumenfeld et al., 2009). These studies support the idea that convulsions arise as a consequence of both cortical and subcortical activity (Gale 1992; Blumenfeld 2002), so that inhibition of activity in either area could suppress convulsions.

Electrographic neonatal seizures frequently have no clinical manifestations, a phenomenon referred to as electroclinical dissociation or uncoupling (Boylan et al., 2002; Castro, Jr. et al., 2005; Connell et al., 1989; Painter et al., 1999; Rennie and Boylan, 2003). Phenobarbital, an allosteric modulator of GABA_{A} R (Twyman and Macdonald 1989), is the drug of choice for treating neonatal seizures. Video-EEG studies have demonstrated that phenobarbital inhibits electrographic seizure activity much less effectively than clinically apparent convulsive activity. This differential efficacy exacerbates electroclinical dissociation (Clancy et al.,

1988; Connell et al., 1989; Rennie, 1997; Scher et al., 2003) so that the incidence of electroclinical dissociation in neonates is 80% after anticonvulsive treatment (Boylan et al., 1999; Boylan et al., 2002; Murray et al., 2008; Scher et al., 2003; Weiner et al., 1991).

To gain insight into mechanisms of electroclinical dissociation and its exacerbation by phenobarbital, we tested the hypotheses that the neocortex and subcortical structures have different $[Cl^-]_i$ during postnatal development using the genetically expressed Cl-sensitive dual wavelength fluorescent protein Clomeleon (Kuner and Augustine, 2000; Berglund et al. 2006). We then tested whether these regions have oppositely directed responses to GABA_AR agonists and phenobarbital, and whether bumetanide, an NKCC1 blocker, preferentially alters the responses to GABA in cortical areas expressing high levels of NKCC1.

Results

Ventroposterior thalamus has lower $[Cl^-]_i$ than the neocortex during early post-natal development

The differences in KCC2 and NKCC1 expression between neurons in the thalamus vs. neocortex suggest that resting neuronal $[Cl^-]_i$ will also be different in these two structures (Wang et al., 2002; Yamada et al., 2004). Gramicidin perforated patch recording is routinely used to measure $[Cl^-]_i$. However, the membrane pores formed by gramicidin, while impermeable to Cl^- , allow the flux of Na^+ which can alter NKCC1 activity because this transporter relies on the transmembrane Na^+ gradient for its function (Brumback and Staley, 2008). In addition, this technique is time consuming which limits the number of neurons that can be sampled. To circumvent these problems, we tested whether $[Cl^-]_i$ is higher in the neocortex than the ventroposterior (VP) thalamus during early development by non-invasively measuring neuronal $[Cl^-]_i$ in hundreds of cells with single cell resolution using two-photon imaging of Clomeleon, an optogenetic Cl^- indicator. In CML-1 mice, Clomeleon is expressed in both the neocortex and thalamus of mice (Berglund et al., 2006; Kuner and Augustine, 2000). Clomeleon is a dual wavelength fluorophore, and the fluorescence ratio provides a quantitative readout of ionic concentration that is independent of indicator intensity (Bright et al., 1989). These features made it feasible to measure $[Cl^-]_i$ in hundreds of cells simultaneously per slice.

We imaged the neocortical layers IV and V and VP thalamus at P5-6, the earliest age at which there was sufficient expression of Clomeleon. Two main findings were observed: first, $[Cl^-]_i$ was widely distributed in both structures at P5-6, P10-11, P15-16 and P20 (Fig. 1A and B). Second, neurons in the VP thalamus always had a significantly lower $[Cl^-]_i$ than in the neocortex (Fig. 1C; Table 1). At P5-6, thalamus $[Cl^-]_i$ was 15.1 ± 1.01 mM ($n=8,950$ cells, 13 slices) compared to 22.1 ± 1.03 mM in neocortex ($n=968$ cells, 11 slices; $p < 0.001$, Wilcoxon-Mann-Whitney test; Table 1). This difference between neocortex and thalamus $[Cl^-]_i$ persisted at P10-11, at P15-16 and P20 (Fig. 1C; Table 1). $[Cl^-]_i$ progressively decreased in both structures during development (Fig. 1C). In addition to the $[Cl^-]_i$ being different in these two structures, the raw data (the measured YFP/CFP ratios) on which the $[Cl^-]_i$ values were calculated and that are independent of Cl^- calibration, were also statistically different between thalamus and neocortex during the different ages studied, ($p < 0.001$ for each age; Wilcoxon-Mann-Whitney test). The differences in $[Cl^-]_i$ are consistent with the different patterns of KCC2 and NKCC1 expression in both structures (Wang et al., 2002), and support the idea of a caudal-rostral pattern of maturation of neuronal Cl^- transport (Stein et al. 2004).

GABA effects are inhibitory in ventroposterior thalamus but excitatory in the neocortex during early development

Our results indicate a lower $[Cl^-]_i$ in thalamus than neocortex, yet GABA actions depend on the relation between RMP and E_{GABA} , which is mainly determined by $[Cl^-]_i$. This relationship is surprisingly difficult to measure (Tyzio et al., 2003) due to the aforementioned difficulties with the influence of direct recording techniques on the neurons' internal ionic milieu. To avoid this problem, we used extracellular multi-unit activity (MUA) recordings that do not alter the intracellular milieu yet provide a direct measure of the net effect of GABA_AR activation on the frequency of network action potentials (Cohen and Miles, 2000; Dzhalal and Staley, 2003). MUA were recorded in rat VP thalamus at early ages (P3-4 and P7-8) in the presence of 2 mM kynurenic acid to block all ionotropic glutamate receptors. Isoguvacine (ISO; 10 μ M), a GABA_AR agonist, induced a significant initial decrease in MUA frequency at P3-4 in 86% of the slices (6/7 slices; Fig. 2). This decrease indicates that the net effect of GABA_AR activation was inhibitory in the thalamus. The inhibitory effects of isoguvacine persisted in 100% of the slices at P7-8 ($n=5$; $p=1$ Fisher's exact test between P3-4 and P7-8; Fig. 2). In contrast, isoguvacine induced an initial increase in MUA in the rat neocortex at P9-10 in 89% of the slices (8/9 slices), an increase that is consistent with an excitatory net effect of GABA_AR activation (Fig. 2). We were unable to record spontaneous MUA in the rat neocortex at earlier ages, which precluded the determination of GABA_AR agonist effects on MUA frequency. However, we were able to measure $[Cl^-]_i$ directly in neocortical neurons at these ages.

Figure 2 also demonstrates a late decrease in MUA in some of the neocortical recordings. We have previously demonstrated that ion flux due to persistent GABA_AR activation by exogenously applied agonists rapidly overcomes NKCC1 transport capacity (Brumback and Staley, 2008), so that E_{Cl} equilibrates near RMP. Under these conditions, GABA_AR activation is shunting and inhibitory (Mann and Paulsen, 2007). For this reason, we only analyzed the initial response to isoguvacine.

In summary, the MUA experiments demonstrate that the actions of GABA during early development are inhibitory in the thalamus while mainly excitatory in the neocortex. These results are consistent with the $[Cl^-]_i$ measurement obtained through Clomeleon. Therefore, if GABA has more inhibitory effects in the thalamus, we hypothesized that phenobarbital, a GABA_AR positive modulator (Twyman and Macdonald 1989), will be more effective in decreasing epileptiform activity in this structure than the neocortex. We turned to the thalamo-cortical preparation as an ideal preparation to study a synaptically connected sub-cortical (VP thalamus) and cortical (neocortex layer IV/V) structure.

Thalamo-cortical epileptiform activity induced in early (P9-10) development

Thalamo-cortical slices have been used to study the effect of anticonvulsive drugs in the adult brain (Zhang et al., 1996; Zhang and Coulter, 1996). Because of the observed differences in neuronal $[Cl^-]_i$ in the thalamus and neocortex during early development, we took the advantage of thalamo-cortical slices to study the effects of phenobarbital, an allosteric GABA_AR modulator (Macdonald and Twyman, 1992) and the most commonly used anticonvulsive drug used in neonatal seizure treatment (Carmo and Barr, 2005), in these interconnected brain structures. This preparation allowed us to measure epileptic activity in synaptically linked cortical and subcortical structures as a test of our hypothesis regarding the mechanisms of electroclinical dissociation. Epileptiform activity was recorded from rat thalamo-cortical slices (P9-10) prepared using a modification of the Agmon and Connors (1991) procedure (See methods, Fig. 3A). Epileptiform activity was not sufficiently stable at earlier postnatal ages, precluding their study. Synchronized epileptiform activity in the neocortex and thalamus was recorded during perfusion of 0 $MgCl_2$ (low- Mg^{2+}) aCSF (Fig. 3B and C). The broadband (1–

500 Hz) power of the extracellular field potential recordings was Fig 4C and D, as well as Fig. 3D for a shorter time span of signal power calculation). This approach allowed us to measure the power of the epileptiform activity as a function of time (Dzhala et al. 2005). At P9-10, epileptiform activity simultaneously recorded in thalamus and neocortex was stable for 90 minutes, and an analysis of variance every 10 minutes confirmed no change in the signal power over the entire recording (Fig. 3D and E). Therefore, we used this preparation to study the effects of phenobarbital in the synaptically connected thalamus and neocortex as early as P9-10.

Thalamo-cortical differences in neuronal $[Cl^-]_i$ persist during seizure activity

Steady state thalamo-cortical differences in neuronal $[Cl^-]_i$ (Figure 1) and steady-state thalamo-cortical differences in the effects of GABA_AR activation (Figure 2) support the hypothesis that there are corresponding differences in the effects of positive allosteric modulators of GABA_AR such as phenobarbital (Twyman and Macdonald, 1989). However, activity-dependent increases in neuronal $[Cl^-]_i$ have been well observed in a number of preparations (Misgeld et al., 1986; Huguenard and Alger, 1986; Staley and Proctor, 1999) and sustained increases in neuronal $[Cl^-]_i$ have been observed in immature hippocampal neurons following trains of action potentials (Fiumelli et al., 2005; Brumback and Staley, 2008) and seizure activity (Khalilov et al. 2003). To ascertain that the relationship between thalamic and cortical neuronal $[Cl^-]_i$ were not changed during seizure activity, we repeated the Clomeleon imaging studies illustrated in Figure 1 during seizure activity induced by low Mg^{2+} aCSF in P9-10 thalamo-cortical slice preparations as illustrated in Figure 3. Extracellular field potential recordings and two-photon confocal imaging of Clomeleon were performed in the neocortex layer IV/V and ventro-posterior thalamus either separately (n=5) or simultaneously (n=3). $[Cl^-]_i$ was measured every 10 min before and after onset of epileptiform activity. Recurrent interictal and ictal-like epileptiform discharges were detected in all neocortical recordings (n=5) and in two out of four recordings in the thalamus. In two more recordings from the thalamus application of low Mg^{2+} aCSF induced only a progressive increase in action potential frequency (not shown). During seizure activity, $[Cl^-]_i$ in cortical neurons (Fig. 4A, C) increased more than thalamic $[Cl^-]_i$ (Fig. 4B, D) and the thalamocortical differences were stably maintained throughout one hour of recurrent interictal and ictal-like epileptiform activity (Fig. 4E). Twenty minutes after onset of recurrent epileptiform discharges $[Cl^-]_i$ was 14 ± 1 mM above the resting chloride level ($p < 0.05$ vs baseline $[Cl^-]_i$, ANOVA followed by Tukey's means comparison test, $n = 268$ neurons in 3 experiments) in the neocortex and 0.5 ± 0.2 mM ($p > 0.05$; $n = 348$ cells in two slices) above the resting chloride level in the thalamus. One hour after onset of seizures, corresponding $[Cl^-]_i$ rise was 26 ± 1.3 mM ($p < 0.05$) in the neocortex and 4.2 ± 0.2 mM ($p < 0.05$) in the thalamus. Thus seizures enhance rather than diminish thalamo-cortical differences in neuronal $[Cl^-]_i$.

Phenobarbital is more effective in decreasing epileptiform activity in thalamus than neocortex in early development

Extracellular MUA recordings were recorded after a period of stable epileptiform activity (low- Mg^{2+}) of at least 30 minutes duration. Baseline control recordings consisted of a stable epileptiform activity for at least 20 min after which phenobarbital (100 μ M) was perfused (Fig. 5A, B and C). The efficacy of phenobarbital (PB) was determined by comparing the mean signal power during the same time windows between thalamus and neocortex and equal length epochs between control and drug perfusion periods. Consistent with the regional differences in $[Cl^-]_i$ and the effects of GABA_AR activation described above, phenobarbital statistically decreased epileptiform power in the thalamus (CON: 0.246 ± 0.03 mV²·Hz, PB: 0.151 ± 0.02 mV²·Hz; $n=9$; $p < 0.001$, paired t -test; PB/CON: 0.62 ± 0.04) but failed to do so in the neocortex (CON: 0.944 ± 0.22 mV²·Hz, PB: 0.915 ± 0.23 mV²·Hz; $n=9$; $p=0.838$ paired t -test; PB/CON: 1.01 ± 0.16 ; Fig. 5D and E). A decrease in ictal power occurred in 9/9 thalamic recordings and only in 3/9 neocortical recordings.

4-Aminopyridine, a voltage gated K^+ channel blocker, is another convulsant frequently used in *in vitro* seizure models. We turned to this seizure model to confirm the differential effects of phenobarbital between thalamus and neocortex recorded in the low- Mg^{2+} model. Results in the presence of 50–100 μM 4-AP (P9-10) were similar to those found in the low- Mg^{2+} model. Phenobarbital reduced the epileptiform power in the thalamus (CON: 0.43 ± 0.03 $mV^2 \cdot Hz$, PB: 0.34 ± 0.03 $mV^2 \cdot Hz$; $n=5$; $p=0.007$, paired *t*-test; PB/CON: 0.77 ± 0.04) but not in the neocortex (CON: 1.03 ± 0.45 $mV^2 \cdot Hz$, PB: 0.81 ± 0.26 $mV^2 \cdot Hz$; $n=5$; $p=0.313$, Wilcoxon Signed Rank test; PB/CON: 0.90 ± 0.07 ; Suppl. Fig. 1).

Next, we studied the effect of phenobarbital on the neocortex and thalamus when the structures were electrically disconnected from each other. We first recorded from coronal brain slices, some of which had their subcortical structures trimmed, in low- Mg^{2+} aCSF. Consistent with the ineffectiveness of phenobarbital on the neocortex in the thalamo-cortical slices, this drug did not change the epileptiform power in isolated rat neocortical slices at P8 (CON: 1.03 ± 0.33 $mV^2 \cdot Hz$, PB: 1.21 ± 0.3 $mV^2 \cdot Hz$; $n=4$; $p=0.224$, paired *t*-test; PB/CON: 1.25 ± 0.11 ; Fig. 6A to C). In addition, phenobarbital also failed to decrease epileptiform activity induced by low- Mg^{2+} recorded in mouse coronal brain slices from P11 Clomeleon mice (CON: 1.66 ± 0.4 $mV^2 \cdot Hz$, PB: 2.13 ± 0.35 $mV^2 \cdot Hz$; $n=5$; $p=0.106$, paired *t*-test; PB/CON: 1.40 ± 0.20 ; Fig. 6D to F). We next recorded from the isolated VP thalamus. Epileptiform activity in the disconnected VP thalamus was obtained using horizontal brain slices from P9-10 rat, with an additional cut through the area of thalamo-cortical fibers in the presence of low- Mg^{2+} plus 100 μM 4-AP. The electrical activity of the neocortex was simultaneously recorded with the thalamus to verify that there was no synchronous activity between both structures. Using this preparation, the thalamus showed independent epileptiform activity from the neocortex. Consistent with the results in thalamo-cortical slices, the electrically disconnected thalamus showed a significant reduction in epileptiform power in the presence of 100 μM phenobarbital (CON: 1.16 ± 0.45 $mV^2 \cdot Hz$, PB: 0.72 ± 0.27 $mV^2 \cdot Hz$; $n=6$; $p=0.031$, Wilcoxon Signed Rank test; PB/CON: 0.65 ± 0.04 ; Fig. 7). Again, the electrically disconnected neocortex showed no decrease in the presence of phenobarbital in these same slices (CON: 0.82 ± 0.32 $mV^2 \cdot Hz$, PB: 0.75 ± 0.26 $mV^2 \cdot Hz$; $n=6$; $p=0.563$, Wilcoxon Signed Rank test; PB/CON: 1.03 ± 0.11).

Therefore, phenobarbital failed to reduce epileptiform activity in the neocortex in both connected thalamo-cortical preparations and when disconnected from thalamus, yet this drug reduced thalamic epileptiform activity in the thalamo-cortical slices and in thalami that were disconnected from the neocortex. This suggests that phenobarbital is ineffective in the neocortex at this early age of development, whether or not the thalamus is connected. Consequently, in the post-natal period, phenobarbital could have regionally specific effects determined by the local neuronal $[Cl^-]_i$.

Bumetanide plus phenobarbital significantly decreased epileptiform activity in the neocortex

There is almost a complete lack of KCC2 expression in the neocortex in early development while the expression of NKCC1 persists as late as the second and third post-natal week (Dzhala et al., 2005; Plotkin et al., 1997). High NKCC1 expression correlates with a higher neuronal $[Cl^-]_i$ during early development (Achilles et al., 2007; Brumback and Staley, 2008; Dzhala et al., 2005; Shimizu-Okabe et al., 2002). Bumetanide is an effective blocker of NKCC1 at low micromolar concentrations (Hannaert et al., 2002; Payne et al., 2003) and has been shown to significantly decrease epileptiform activity in neonatal hippocampus *in vitro* and *in vivo* when combined with phenobarbital (Dzhala et al., 2005; Dzhala et al., 2007) but see (Kilb et al., 2007). Thus, we tested whether bumetanide would decrease the power of the epileptiform activity in the neocortex without altering thalamic epileptiform activity in the combined thalamo-cortical slice preparation.

After eliciting synchronized epileptiform activity in the thalamo-cortical preparation with low-Mg²⁺, 100 μM phenobarbital plus 10 μM bumetanide (PB+BUM) was perfused. In contrast to phenobarbital alone, this drug combination statistically decreased the epileptiform power in the neocortex (CON: 1.3±0.26 mV²·Hz, PB+BUM: 0.41±0.10 mV²·Hz; *n*=8; *p*=0.010, paired *t*-test; PB+BUM/CON: 0.30±0.04), while continuing to decrease the epileptiform power in the thalamus (CON: 0.18±0.03 mV²·Hz, PB+BUM: 0.09±0.01 mV²·Hz; *n*=8; *p*=0.011, paired *t*-test; PB+BUM/CON: 0.58±0.07; Fig. 8). However, in the thalamus, phenobarbital plus bumetanide did not show a further decrease in total power ratio compared to phenobarbital alone (PB/CON: 0.62±0.04, *n*=9; PB+BUM/CON: 0.58±0.07, *n*=8; *p*=0.619, unpaired *t*-test), as would be expected based on the lower [Cl⁻]_i in these neurons. In contrast, phenobarbital plus bumetanide was more effective in the neocortex than phenobarbital alone (PB/CON: 1.01±0.16, *n*=9; PB+BUM/CON: 0.30±0.04, *n*=8; *p*=0.002, Wilcoxon-Mann-Whitney test). Consistent with this result, phenobarbital plus bumetanide statistically decreased the epileptiform power elicited in the neocortex isolated from the thalamus of Clomeleon mice [P9] in the presence of low-Mg²⁺ (CON: 2.46±0.28 mV²·Hz, PB+BUM: 1.1±0.14 mV²·Hz; *n*=8; *p*<0.001, paired *t*-test; PB+BUM: 0.46±0.05; Suppl. Fig. 2). The effectiveness of phenobarbital plus bumetanide in reducing epileptiform activity in the neocortex vs. thalamus further supports a difference in GABAergic maturation in cortical versus subcortical structures.

GABAergic development is similar between the amygdala and thalamus

To provide additional evidence that phenobarbital is effective depending in part on the neuron's [Cl⁻]_i, we repeated the experiments described for neocortex and thalamus in two different regions, the hippocampus and amygdala. The ontogeny of Cl⁻ transport in the amygdala is similar to the thalamus: they both express KCC2 at very early ages during embryonic development with an almost complete absence of NKCC1. In contrast, the ontogeny of hippocampal Cl⁻ transport closely resembles the neocortex (Wang et al., 2002), and the CA3 hippocampal area is well characterized regarding its GABAergic developmental profile and response to anticonvulsants (Ben-Ari et al., 2007; Dzhalala et al., 2007; Dzhalala and Staley, 2003; Quilichini et al., 2003; Rivera et al., 1999; Tyzio et al., 2007). Therefore, we investigated the effects of isoguvacine on MUA frequency recorded in the amygdala (*n. medialis*) at early post-natal days in the presence of kynurenic acid (2 mM) using the hippocampal CA3 region as an internal control when simultaneous recordings in the amygdala and CA3 region could be performed. Similarly to the thalamus, isoguvacine (10 μM) decreased MUA frequency in the rat amygdala at post-natal day 3–4 [P3-4] in 9 out of 11 slices recorded (82%; Suppl. Fig. 3). In contrast, 10 μM isoguvacine increased the frequency of action potentials recorded in the CA3 region of the hippocampus at the same post-natal age in 5 out of 6 slices (83%; Suppl. Fig. 3).

The inhibitory effect of isoguvacine was similar in the amygdala at P7-8 (100%, *n*=7; *p*=0.5 Fisher's exact test between P3-4 and P7-8; Suppl. Fig. 3) while the excitatory effects of isoguvacine persisted in the CA3 region during this same age in 5 out of 6 slices (83%; *p*=1 Fisher's exact test between P3-4 and P7-8; Suppl. Fig. 3).

Phenobarbital is more effective in decreasing epileptiform activity in the amygdala than the CA3 region

Epileptiform activity was induced in rat P4-6 brain slices by perfusing aCSF with low-Mg²⁺. After a control baseline period, 100 μM phenobarbital was perfused. Phenobarbital had a modest, yet significant, decrease in the signal power of the CA3 region (CON: 0.41±0.09 mV²·Hz, PB: 0.31±0.06 mV²·Hz; *n*=11; *p*=0.032, Wilcoxon Signed Rank test; Suppl. Fig. 4). In comparison, phenobarbital statistically decreased the epileptiform signal power in the amygdala (CON: 0.25±0.04 mV²·Hz, PB: 0.14±0.02 mV²·Hz; *n*=8; *p*=0.002, paired *t*-test; Suppl. Fig. 5). Moreover, the phenobarbital effect in the amygdala was more effective than in

the CA3 region when the PB/CON of the signal power in both structures was compared (Amygdala: 0.60 ± 0.06 , $n=8$; CA3: 0.84 ± 0.07 , $n=11$; $p=0.021$, unpaired t -test) which correlates with the inhibitory effect of isoguvacine in the amygdala but not the hippocampus.

These results support a caudal-rostral development of GABAergic activity as thalamus and amygdala share a similar KCC2-NKCC1 expression pattern and hence a more mature GABAergic signaling than the neocortex and hippocampus, which also share a similar NKCC1-KCC2 pattern and more immature GABA effects.

GABA effects are similar between regions of the male and female brain

CA1 pyramidal neurons of female rat pups were shown to have a lower $[Cl^-]_i$ than male pups during early development (Galanopoulou, 2008). We decided to test if sex differences in GABAergic effects were evident in the CA3 region, thalamus and amygdala. The effect of isoguvacine recorded in female rats (P4-6) was comparable to the ones recorded in males (female: [CA3]: 100% of slices increased MUA frequency ($n=6$ slices); [Amygdala]: 100% of slices decreased frequency ($n=7$ slices). [Thalamus]: 83% of slices decreased MUA frequency (5/6 slices); Suppl. Fig. 6). Thus, the effects of isoguvacine did not differ between male and female brains in the recorded regions.

Discussion

Our main findings are: 1) $[Cl^-]_i$ varies substantially between neighboring neurons in both the developing thalamus and neocortex, but the average $[Cl^-]_i$ is significantly lower in thalamic vs. cortical neurons. 2) Phenobarbital is an effective anticonvulsant in the thalamus but not in the neocortex, due to a net inhibitory effect of GABA in the thalamus but an excitatory effect in the neocortex. 3) The combination of bumetanide and phenobarbital is effective in decreasing epileptiform activity in the neocortex while it is not different from phenobarbital alone in the thalamus. Our results support the idea that caudal-rostral $[Cl^-]_i$ maturation determines neuronal responses to GABA and therefore the effects of allosteric modulators of GABA_AR function. Taken together, these differences in $[Cl^-]_i$ comprise a candidate mechanism of electroclinical dissociation of neonatal seizures and the exacerbation of dissociation by GABAergic anticonvulsants.

Measuring neuronal $[Cl^-]_i$

The best methods for measuring neuronal Cl^- are still being established. Approaches include gramicidin perforated patches, which form membrane pores impermeable to anions while allowing the passage of cations (Kyzozis and Reichling, 1995). A disadvantage of this widely used technique is diffusion of Na^+ from the intracellular pipette to the neuron, which alters $[Na^+]_i$, and the driving force for NKCC1-mediated Cl^- transport (Brumback and Staley, 2008; Shimizu-Okabe et al., 2002). Cell-attached patches have also been used to estimate E_{GABA} from the reversals of single-channel currents (Tyzio et al., 2007). These methods are less invasive but they have limited time resolution, and may activate stretch-activated potassium channels near the patch (Hammami et al. 2009). Both patch techniques are time-consuming, so that only limited numbers of neurons can be assayed. Measurement of spontaneous action potential frequency and Clomeleon dye measurements are noninvasive and have the added benefit of recording a significant number of neurons simultaneously (Cohen and Miles, 2000; Dzhalala and Staley, 2003). The large sample sizes reported here provide a new insight into the heterogeneity of the ontogeny of neuronal Cl^- transport not only between but also within regions of the brain. However, action potential measurements do not provide a direct measure of E_{GABA} . Disadvantages of Clomeleon include pH sensitivity, the need for calibration, potential differences in tissue transmission of yellow vs. cyan light, and limitation

to neurons that express the dye. For example, $[Cl^-]_i$ in the amygdala was not imaged due to a null or low expression during early development in CML-1 mice.

Intracellular ionic concentrations are affected by the extracellular concentration of ions as well as substances present in the cerebrospinal fluid. Compared to our results, cortical neurons in brain slices supplied with ketone bodies demonstrated more negative values for E_{GABA} that were dependent on intact HCO_3^-/Cl^- exchange (Zilberter et al., 2009). However, perfusion of high concentrations of a weak acid is a well-established method of acidifying the intracellular compartment (Roos and Boron 1981; Dulla et al., 2009). Independently of metabolic effects, the perfusion of 4 mM of the ketone 3-hydroxybutyrate (pK_a 4.7) by Zilberter et al. would be expected to acidify the neuronal cytoplasm, reducing intracellular HCO_3^- (Roos and Boron 1981). HCO_3^-/Cl^- exchange would then reduce $[Cl^-]_i$ (Romero et al. 2004), producing the observed negative values of E_{Cl} and E_{GABA} and dependence on HCO_3^-/Cl^- exchange.

Neuronal $[Cl^-]_i$ and the expression of Cl^- transporters

The expression of KCC2 is high in the thalamus during the perinatal period, while NKCC1 expression is low (Li et al., 2002; Stein et al., 2004; Wang et al., 2002). In the neocortex, NKCC1 expression is high in the perinatal period and decreases progressively the first two postnatal weeks; conversely, embryonic and early perinatal KCC2 expression is low and increases post-natally (Clayton et al., 1998; Plotkin et al., 1997; Yamada et al., 2004). The expression of KCC2 is negatively correlated with $[Cl^-]_i$, while the expression of NKCC1 is positively correlated with $[Cl^-]_i$ (DeFazio et al., 2000; Hubner et al., 2001; Owens et al., 1996; Rheims et al., 2008a; Sung et al., 2000; Yamada et al., 2004; Zhu et al., 2005). While NKCC1 and KCC2 appear to be the main transporters setting $[Cl^-]_i$ in neurons (Sung et al., 2000; Zhu et al., 2005), other transmembrane chloride pathways may also be involved including NDCBE (Na^+ Driven Chloride Bicarbonate exchanger, also known as SLC4A8; involved in pH regulation) and CLC-2 (Conductive Cl^- channel) (Chen et al., 2008; Gonzalez-Islas et al., 2009; Romero et al., 2004; Staley, 1994; Staley et al., 1996). However, the robust effects of NKCC1 inhibition on the efficacy of GABA-mediated inhibition (Figure 8; Dzhala et al. 2005; Sipila et al. 2006; Brumback and Staley 2008; Rheims et al. 2008b) indicate that NKCC1 is the primary Cl^- accumulator in neocortical and hippocampal neurons. Layer IV/V neocortical $[Cl^-]_i$ was higher than the VP thalamus during early development in agreement with our MUA recordings. The $[Cl^-]_i$ developmental profile in neocortex and thalamus is reminiscent of the development of the visual cortex and the dorsal lateral geniculate nucleus (dLGN) (Ikeda et al., 2003).

While $[Cl^-]_i$ measurements *in vivo* are lacking, bumetanide blocked sharp waves recorded in the hippocampus *in vivo* (Sipila et al., 2006). Sharp waves are analogous to the giant depolarizing potentials (GDPs) recorded in this area *in vitro*, and GDPs are also blocked by bumetanide (Dzhala et al. 2005). This suggests that the higher $[Cl^-]_i$ recorded *in vitro* during early development (Tyzio et al. 2007; Figure 1) is also present *in vivo*. Neonatal seizures occur most commonly several hours after an acute cerebral injury (Tekgul et al., 2006). Hypoxia has been shown to cause both a late increase NKCC1 expression (Yan et al., 2003) and a delayed increase in neuronal $[Cl^-]_i$ (Pond et al. 2006). This increase in $[Cl^-]_i$ may be sufficient to invert the action of GABA and trigger seizures. Seizures themselves may further increase $[Cl^-]_i$, because trains of action potentials have also been demonstrated to cause sustained increases in Cl^- (Fiumelli et al. 2005; Brumback and Staley 2008; Figure 4). Thus in the setting of post-hypoxic seizures in human neonates that express high levels of NKCC1 in cortical neurons (Dzhala et al. 2005), the balance of evidence suggests that GABA_AR activity is excitatory in the cortex during neonatal seizures.

Our measurements revealed a wide distribution of neuronal $[Cl^-]_i$. Our neocortical $[Cl^-]_i$ measurements are similar to previous $[Cl^-]_i$ measurements obtained from different techniques

(Owens et al., 1996; Yamada et al., 2004), yet we demonstrate a wide intra-area variation that is difficult to observe with direct recording methods because of the number of neurons that must be recorded (Ebihara et al. 1995). The remarkable inter-neuron variance in $[Cl^-]_i$ implies that very large numbers of neurons should be sampled in order to accurately assess neuronal $[Cl^-]_i$. This $[Cl^-]_i$ variation suggests that some neurons will have E_{GABA} above RMP while in others it will be below RMP. Therefore, the net effect of drugs that modulate GABAergic transmission will depend on the proportion as well as the classes of neurons having excitatory and inhibitory actions of GABA.

The problem of electroclinical dissociation

The EEG preferentially records neocortical activity (Marks et al., 1992). As described in the introduction, convulsions are the motor manifestation of cortical seizure activity, however this activity, recoded electrographically, is neither necessary nor sufficient to produce convulsive activity in human neonates (Mizrahi and Kellaway, 1987; Connell et al., 1989; Scher et al. 2003; Murray et al. 2008). Thus many neonates have convulsions with no cortical EEG correlate (Mizrahi and Kellaway, 1987), and neonates frequently manifest electrographic seizure activity without convulsive activity (electroclinical dissociation or uncoupling; Scher et al. 2003). The prominent role of subcortical networks in the production of convulsive activity (Gale, 1992; White and Price, 1993; Blumenfeld, 2009) frame the hypothesis that selective inhibition of subcortical structures could suppress convulsive activity but not electrographic cortical seizure activity in neonates, and this selective inhibition could arise from the differential neuronal Cl^- transport (Stein et al. 2004), $[Cl^-]_i$ (Figure 1), and consequent effects of $GABA_A$ R activation (Figure 2) in these structures.

The modulatory effects of anticonvulsant drugs

The low efficacy of phenobarbital in suppressing cortical vs. thalamic epileptiform activity in our experiments comprises a candidate mechanism for the exacerbation of electroclinical dissociation by phenobarbital. Phenobarbital exhibited the same efficacy in the perinatal thalamus as in adult *in vitro* thalamo-cortical preparations (Zhang and Coulter, 1996) as well as *in vivo* (Hosford et al., 1997), and this efficacy was not improved by bumetanide, supporting the idea that in the perinatal period, thalamic neurons have developed mature patterns of neuronal Cl^- transport (Stein et al. 2004), $GABA_A$ signaling (Figure 2), and anticonvulsant responses to phenobarbital (Figure 5). We used the thalamus as a model subcortical structure because of the high correlation between thalamic activation and convulsive activity (White and Price 1993; Blumenfeld 2009) as well as the high expression of Clomeleon in the perinatal CML1 mouse (Berglund et al. 2008). However, electroclinical dissociation could also arise as a consequence of a higher efficacy of phenobarbital in any subcortical network involved in transmission of convulsive activity, including the spinal cord, a region with the earliest KCC2 expression (Stein et al. 2004).

Although the anticonvulsant effects of phenobarbital in human neonates are poor when measured electrographically, they are not absent (Painter et al. 1999). Similarly, we observed modest but significant anticonvulsant effects in our experiments in area CA3, even though GABA appeared excitatory in this region based on the net increase in action potential frequency in response to perfusion a $GABA_A$ R agonist. There are several reasons why phenobarbital could exhibit anticonvulsant activity in structures with excitatory responses to $GABA_A$ R activation. During seizure activity, paroxysmal depolarizing shifts in the membrane potential (PDS) result in membrane potentials that are very positive to the GABA reversal potential, even in immature neurons. Thus, $GABA_A$ R activation can repolarize the membrane potential relative to the PDS even though E_{GABA} is more positive than RMP. Additionally, high concentrations of GABA agonists or allosteric modulators may result in Cl^- fluxes through the $GABA_A$ R that are sufficiently large and prolonged to change $[Cl^-]_i$ and so shift E_{GABA} toward

RMP (Brumback and Staley, 2008; Proctor and Staley, 1999), in which case GABA_A receptor activation would provide effective shunting inhibition. Further, in a network of neurons, a variety of E_{GABA_s} are apparent (Fig. 1). Thus, the effect of phenobarbital on the network is even less predictable than in an individual neuron. Finally, phenobarbital may have other anticonvulsant actions besides allosteric modulation of the GABA_A receptor (Kitayama et al. 2002). These issues may underlie the sometimes conflicting results of different investigators regarding the anticonvulsant efficacy of allosteric modulators of GABA_AR (Dzhala et al., 2005; Dzhala et al., 2007; Kilb et al., 2007; Wells et al., 2000). Our results provide evidence that phenobarbital's anticonvulsant efficacy parallels the efficacy of GABA_AR-mediated inhibition (Dzhala et al., 2005; Quilichini et al., 2003).

To our knowledge, this is the first report to show the differential effect of phenobarbital in two synaptically connected structures that also demonstrate differences in [Cl⁻]_i. We recorded the epileptiform activity of a thalamo-cortical slice for the first time, as far as we know, from P9-10 rat pups. The different effects of phenobarbital on both structures correlates to the opposite effects of isoguvacine on MUA frequency, the differences in neuronal [Cl⁻]_i, and the previously reported differences in KCC2 vs. NKCC1 expression in these two areas. This combined preparation provides experimental support for the hypothesis that exacerbation of electroclinical dissociation arises from the selective anticonvulsant efficacy of phenobarbital in subcortical vs. cortical regions.

Bumetanide and its potential role in electroclinical dissociation

Drugs that reduce the [Cl⁻]_i by blocking NKCC1 activity, e.g. bumetanide, improve the electroencephalographic anticonvulsive effects of phenobarbital in vitro and in vivo (Dzhala et al., 2005; Dzhala et al., 2008). In Swiss mice, bumetanide alone decreased seizure activity in the neocortex during early development (Rheims et al., 2008b) and the effect of bumetanide is synergistic with phenobarbital (Dzhala et al., 2008). This drug combination could be of significant impact in the human neonate, and therefore we studied these two drugs in conjunction. This synergistic effect statistically decreased the epileptiform activity in the neocortex, whereas phenobarbital alone did not. The anticonvulsant effects of phenobarbital were not enhanced by bumetanide in the thalamus. Thus the anticonvulsant effect of bumetanide would be more evident electrographically rather than clinically: neonates whose convulsions were already suppressed by selective effects of Phenobarbital on subcortical networks could not manifest additional reductions in convulsions, but electrographic seizure activity could be reduced.

Neuronal NKCC1 is upregulated in adult patients suffering from chronic temporal lobe epilepsy, so bumetanide might be helpful in this population (Huberfeld et al., 2007; Palma et al., 2006). Post-hypoxic increases in NKCC1 expression (Yan et al. 2003) and neuronal chloride are seen in adult neurons experimentally (Pond et al. 2006), and electroclinical dissociation has recently been observed in critically ill adult patients (Oddo et al. 2009), but it is not known whether pharmacological inhibition of NKCC1 is useful in this setting.

KCC2 and NKCC1 expression pattern in the developing human parietal cortex is similar to the levels found in rat neocortex (Dzhala et al., 2005), although the pattern of expression of these transporters in subcortical structures has not been studied in humans. Bumetanide has been extensively studied as a diuretic in human neonates (Lopez-Samblas et al., 1997; Sullivan et al., 1996). More recent experimental indicate that long-term suppression of NKCC1 activity and chronic KCC2 over-expression produce alterations in migration patterns of neocortical principal neurons and their dendritic length (Ge et al. 2006; Cancedda et al., 2007; Wang and Kriegstein, 2008). However, long-term changes in brain activity due to NKCC1 block during seizures have not been studied. Most human neonates would not require long-term treatment with bumetanide; the majority of neonatal seizures are an acute reaction to brain injury (Tekgul

et al. 2006), and under these circumstances anticonvulsant treatment can usually discontinued after the first week of life (Carmo et al. 2005). Recently, bumetanide treatment was reported to decrease seizure duration and frequency in a 6 week baby girl with anticonvulsant-resistant status epilepticus secondary to meningitis (Kahle et al., 2009). A pilot trial of bumetanide for neonatal seizure treatment is currently under way (Clinicaltrials.gov # NCT00830531).

In conclusion, our results support the hypothesis of a caudal-rostral functional maturation of GABA actions and provide a candidate pathophysiological mechanism of neonatal electroclinical dissociation as well as a pharmacotherapy that could be beneficial in this condition.

Experimental Procedures

Slice preparation

Post-natal (ages: P3–10) male (female where indicated) Sprague-Dawley rats and CLM1 Clomeleon mice (P5-P20; C57bl/6 background) were anaesthetized and decapitated according to a protocol approved by the Massachusetts General Hospital Center for Comparative Medicine. The brain was removed and placed in ice-cold artificial cerebrospinal fluid (aCSF) containing (mM): NaCl (120), KCl (3.3), CaCl₂ (1.3), MgCl₂ (2), NaH₂PO₄ (1.25), NaHCO₃ (25) and D-glucose (10) with pH 7.3–7.4 when bubbled with 95% O₂ and 5% CO₂. Coronal and horizontal brain slices, 450–500 μm thick, were cut with a Leica VT1000S Vibratome (Leica Microsystems, Wetzlar, Germany) in aCSF containing 2 mM kynurenic acid (Sigma; St. Louis, MO). In a subset of coronal slices, subcortical structures were trimmed. Thalamo-cortical brain slices were obtained by modifying the procedure by Agmon and Connors (1991) as follows: after exposing the brain by removing the parietal, temporal and occipital bones, a 45° angle coronal cut was performed before removing the brain from the base of the cranium and its rostral end was glued to the vibratome dish. Slices were placed into an interface holding chamber kept at room temperature and stored for at least 1 h before being transferred to the recording chamber.

Electrophysiology

Brain slices were placed in an upright microscope (Zeiss, Axioskop; Thornwood, NY) perfused with aCSF (0.5 mM MgCl₂ to increase spontaneous activity when recording MUA) held at 32–34 °C and aerated with 95% O₂-5% CO₂ (flow rate of 5–8 ml/min). Tungsten coated electrodes were placed in either neocortex layer IV/V, CA3 region of the hippocampus, amygdala (*n. medialis*), and thalamus (ventroposterior nucleus). Recordings were obtained through a CyberAmp 320 amplifier (Molecular Devices, Sunnyvale, CA) with a x10,000 gain, digitized at 10 KHz with a DigiData 1321A (Molecular Devices) and recorded with pClamp (Molecular Devices). Epileptiform activity was induced by perfusing the brain slices with aCSF containing 0 MgCl₂ (low-MgCl₂) or 4-Aminopyridine (4-AP) and recordings were started after 30 min of consistent epileptiform activity. Drugs were perfused as indicated.

Imaging

Two-photon imaging was performed using a Fluoview 1000MPE with pre-chirp optics and a fast acousto-optical modulator (AOM) mounted on a Olympus BX61WI upright microscope (Olympus Optical) using a 20x water immersion objective (NA 0.95; Suppl. Fig. 7A). A mode-locked Ti:Sapphire laser (MaiTai, Spectra-Physics, Fremont, CA) generated two-photon fluorescence with 860 nm excitation. CFP and YFP filters (340–480 and 500–540 nm respectively) and two photomultiplier tubes (Hamamatsu Photonics) were used to simultaneously acquiring CFP and YFP signal. Three dimensional stacks (3D) were imaged. Slices were perfused with aCSF held at 32–34 °C and aerated with 95% O₂-5% CO₂.

Analysis

1) Multi-unit activity detection and analysis—Recordings were high-passed filtered at 10 Hz. Events were detected by MiniAnalysis (Synaptosoft, Inc., Fort Lee, NJ). Isoguvacine effect was determined by using a peak function running under Origin (OriginLab Corporation, Northampton, MA) based on the following equation:

$$y=y_0+Ae^{(-e^{-(x-xc)-z+1})} \quad (1)$$

$$z=(x-xc)/w \quad (2)$$

where y_0 is the offset, A is amplitude, xc is the center and w is the width. The first peak (either negative or positive) after perfusion of isoguvacine was taken as the effect of this drug.

2) Epileptiform activity analysis—A custom-written macro running under IGOR Pro v6 (Lake Oswego, OR) was used. Briefly, the complete trace was loaded and down sampled to 2 KHz. For each epoch of 30 sec, its mean value was subtracted and Fast Fourier Transformed using Hann window apodization. Next, the FFT was smoothed with a median window of 7 points, divided by the total number of points, and the signal power area (1–500 Hz) was calculated (Supp. Fig. 4B and C). The wide-band power is mathematically identical to the square of the field potential, and thus represents an unbiased measure to quantify seizure activity (e.g. Sup. Fig. 2; Dzhala et al. 2005, 2008). The wide-band power is proportionately affected by the frequency of discharge and the fraction of the population participating in the discharge. Finally, the mean signal power during equal control and drug condition epochs was calculated. This method allowed us to address the combined effect of drugs on the frequency and power of the epileptiform activities. Graphs display the signal power in the EEG band (1–160Hz) (Bragin et al., 1999; Bragin et al., 2004; Khosravani et al., 2005).

3) $[Cl^-]_i$ determination—Quantitative measurements on 3D stacks were performed using Image J (National Institutes of Health, freeware) offline. The CFP and YFP images were loaded and their respective background value was subtracted for the 3D volume. Next, a median filtered was applied to all of the 3D planes. Cells were visually identified and a region of interest (ROI) was drawn around the cell bodies and the ratio of the YFP/CFP fluorescence intensity was measured. Each cell's YFP/CFP ratio was converted into $[Cl^-]_i$ by the following equation:

$$[Cl^-]_i = K'_D \cdot \frac{(R_{max} - R)}{(R - R_{min})} \quad (3)$$

where K'_D is the apparent dissociation constant, R_{max} is the ratio when Clomeleon is not bound by Cl^- and R_{min} when it is completely quenched by F^- (Berglund et al., 2008; Kuner and Augustine, 2000). These values were calculated from the calibration of $[Cl^-]_i$ in acute slices (Suppl. Figure 7B). The mean of the logarithmic value of the $[Cl^-]_i$ was used in every case, as the ion concentration follows a log-normal distribution. E_{Cl} was calculated using the Nernst equation setting the temperature variable at 33 °C.

4) Calibration of Clomeleon—Acute brain slices of the neocortex (P11-15) were used to calibrate the YFP/CFP intensity to $[Cl^-]$ (Berglund et al., 2008; Krapf et al., 1988). Briefly, acute brain slices were exposed to the K^+/H^+ ionophore nigericin (50 μ M) and the Cl^-/OH^- antiporter tributyltin chloride (100 μ M) in the presence of 20, 80 and 123 mM $[Cl^-]_o$. Neurons

that experienced a change in YFP/CFP intensity to each $[Cl^-]_o$ were used for the calibrations. The data points obtained with the different $[Cl^-]_o$ are described by the ratiometric function:

$$R = \frac{K'_D \cdot R_{max} + [Cl^-] \cdot R_{min}}{[Cl^-] + K'_D} \quad (4)$$

R_{max} and K'_D were free parameters, while R_{min} was determined by quenching Clomeleon with 123 mM F^- (Duebel et al., 2006; Kuner and Augustine, 2000). With single-cell resolution, we calculated R_{max} and K'_D for 47 individual neurons that we were able to follow across all calibration conditions. The K'_D was 91 ± 5.43 mM, R_{max} was 1.026 and R_{min} was 0.268 (Suppl Fig. 7B). To determine if the Cl^- calibration is consistent with the expected $[Cl^-]_i$ values, we perfused 500 μ M GABA onto P31 neocortical pyramidal cells. We observed an increase in $[Cl^-]_i$ in cells with low initial $[Cl^-]_i$ while the opposite was recorded in neurons with high initial $[Cl^-]_i$ (Suppl. Fig. 7D,E). While Clomeleon is sensitive to intracellular pH (pH_i) at high $[Cl^-]$ (150 mM), it is not pH sensitive at lower $[Cl^-]$ (10 mM). Changes of 0.2 pH units would cause the apparent $[Cl^-]_i$ to change a few millimolars for $[Cl^-]$ smaller than 50 mM and produce large deviations at 150 mM (Kuner and Augustine, 2000). However, this sensitivity of Clomeleon to pH should not affect our $[Cl^-]_i$ determination as pH is tightly regulated in neurons (Bonnet et al., 1998) and we performed all of our experiments in resting neurons bathed in CO_2 - HCO_3^- buffered solution which prevents pH_i changes. The pH_i could be of concern in *in vivo* preparations, where the pH is not directly controlled; or in experiments known to change pH_i . Moreover, there were no exchanges of extracellular solutions or drug perfusion that could alter pH_i . Even though we were careful in the calibration of Clomeleon, we also included the statistics on the actual YFP/CFP ratios, which are independent of Cl^- calibration.

Statistics

The Shapiro-Wilk test was used to determine if the data followed a Gaussian distribution. The parametric Student *t*-test (paired and unpaired, two-tail) was used if the data were normally distributed while the Wilcoxon-Mann-Whitney test (unpaired data, two-tail) and Wilcoxon Signed Rank test (paired data, two-tail) was used for non-Gaussian distributions. Analysis of variance (one-way ANOVA) was performed when measuring multiple conditions. Statistical analysis of the linear regression slopes was done using a Student *t*-test (Zar, 1999). Fisher's exact test (two-tail) was used when comparing proportions. Statistical significance was set to $p < 0.05$. Values are expressed as mean \pm standard error of the mean (SEM).

Drugs

Isoguvacine was obtained from Tocris (Ellisville, MO). Kynurenic acid, phenobarbital, nigericin, tributyltin chloride, 4-AP and bumetanide were obtained from Sigma (St. Louis, MO). Bumetanide was dissolved in 100% ethanol and made fresh every day.

Supplementary Material

Refer to Web version on PubMed Central for supplementary material.

Acknowledgments

To the Staley lab for helpful discussion. This work was supported by the American Epilepsy Society (JG), NIH NS580752 (KVK), NIH NS040109 (KJS) and NIH EB000768 (BJB).

Reference List

- Achilles K, Okabe A, Ikeda M, Shimizu-Okabe C, Yamada J, Fukuda A, Luhmann HJ, Kilb W. Kinetic properties of Cl uptake mediated by Na⁺-dependent K⁺-2Cl cotransport in immature rat neocortical neurons. *J Neurosci* 2007;27:8616–8627. [PubMed: 17687039]
- Agmon A, Connors BW. Thalamocortical responses of mouse somatosensory (barrel) cortex in vitro. *Neuroscience* 1991;41:365–379. [PubMed: 1870696]
- Ben-Ari Y, Gaiarsa JL, Tyzio R, Khazipov R. GABA: a pioneer transmitter that excites immature neurons and generates primitive oscillations. *Physiol Rev* 2007;87:1215–1284. [PubMed: 17928584]
- Berglund K, Schleich W, Krieger P, Loo LS, Wang D, Cant NB, Feng G, Augustine GJ, Kuner T. Imaging synaptic inhibition in transgenic mice expressing the chloride indicator, Clomeleon. *Brain Cell Biol.* 2008
- Blumenfeld H. The thalamus and seizures. *Arch Neurol* 2002;59:135–137. [PubMed: 11790241]
- Blumenfeld H, Varghese GI, Purcaro MJ, Motelow JE, Enev M, McNally KA, Levin AR, Hirsch LJ, Tikofsky R, Zupal IG, Paige AL, Spencer SS. Cortical and subcortical networks in human secondarily generalized tonic-clonic seizures. *Brain* 2009;132:999–1012. [PubMed: 19339252]
- Bonnet U, Wiemann M, Bingmann D. CO₂/HCO₃⁻-withdrawal from the bath medium of hippocampal slices: biphasic effect on intracellular pH and bioelectric activity of CA3-neurons. *Brain Res* 1998;796:161–170. [PubMed: 9689466]
- Boylan GB, Pressler RM, Rennie JM, Morton M, Leow PL, Hughes R, Binnie CD. Outcome of electroclinical, electrographic, and clinical seizures in the newborn infant. *Dev Med Child Neurol* 1999;41:819–825. [PubMed: 10619280]
- Boylan GB, Rennie JM, Pressler RM, Wilson G, Morton M, Binnie CD. Phenobarbitone, neonatal seizures, and video-EEG. *Arch Dis Child Fetal Neonatal Ed* 2002;86:F165–F170. [PubMed: 11978746]
- Bragin A, Engel J Jr, Wilson CL, Fried I, Buzsaki G. High-frequency oscillations in human brain. *Hippocampus* 1999;9:137–142. [PubMed: 10226774]
- Bragin A, Wilson CL, Almajano J, Mody I, Engel J Jr. High-frequency oscillations after status epilepticus: epileptogenesis and seizure genesis. *Epilepsia* 2004;45:1017–1023. [PubMed: 15329064]
- Bright GR, Fisher GW, Rogowska J, Taylor DL. Fluorescence ratio imaging microscopy. *Methods Cell Biol* 1989;30:157–192. [PubMed: 2648109]
- Brumback AC, Staley KJ. Thermodynamic regulation of NKCC1-mediated Cl⁻ cotransport underlies plasticity of GABA(A) signaling in neonatal neurons. *J Neurosci* 2008;28:1301–1312. [PubMed: 18256250]
- Cancedda L, Fiumelli H, Chen K, Poo MM. Excitatory GABA action is essential for morphological maturation of cortical neurons in vivo. *J Neurosci* 2007;27:5224–5235. [PubMed: 17494709]
- Carmo KB, Barr P. Drug treatment of neonatal seizures by neonatologists and paediatric neurologists. *J Paediatr Child Health* 2005;41:313–316. [PubMed: 16014133]
- Castro C Jr, Hernandez Borges AA, Domenech ME, Gonzalez CC, Perera SR. Midazolam in neonatal seizures with no response to phenobarbital. *Neurology* 2005;64:876–879. [PubMed: 15753426]
- Chen LM, Kelly ML, Parker MD, Bouyer P, Gill HS, Felie JM, Davis BA, Boron WF. Expression and localization of Na-driven Cl-HCO₃⁻ exchanger (SLC4A8) in rodent CNS. *Neuroscience* 2008;153:162–174. [PubMed: 18359573]
- Clancy RR, Legido A, Lewis D. Occult neonatal seizures. *Epilepsia* 1988;29:256–261. [PubMed: 3371282]
- Clayton GH, Owens GC, Wolff JS, Smith RL. Ontogeny of cation-Cl⁻ cotransporter expression in rat neocortex. *Brain Res Dev Brain Res* 1998;109:281–292.
- Cohen I, Miles R. Contributions of intrinsic and synaptic activities to the generation of neuronal discharges in in vitro hippocampus. *J Physiol* 2000;524(Pt 2):485–502. [PubMed: 10766928]
- Connell J, Oozeer R, de VL, Dubowitz LM, Dubowitz V. Clinical and EEG response to anticonvulsants in neonatal seizures. *Arch Dis Child* 1989;64:459–464. [PubMed: 2730114]
- DeFazio RA, Keros S, Quick MW, Hablitz JJ. Potassium-coupled chloride cotransport controls intracellular chloride in rat neocortical pyramidal neurons. *J Neurosci* 2000;20:8069–8076. [PubMed: 11050128]

- Duebel J, Haverkamp S, Schleich W, Feng G, Augustine GJ, Kuner T, Euler T. Two-photon imaging reveals somatodendritic chloride gradient in retinal ON-type bipolar cells expressing the biosensor Clomeleon. *Neuron* 2006;49:81–94. [PubMed: 16387641]
- Dulla CG, Frenguelli BG, Staley KJ, Masino SA. Intracellular Acidification Causes Adenosine Release during States of Hyperexcitability in the Hippocampus. *J Neurophysiol.* 2009;101:1152–1162. [PubMed: 1906952008]
- Dzhala VI, Brumback AC, Staley KJ. Bumetanide enhances phenobarbital efficacy in a neonatal seizure model. *Ann Neurol* 2008;63(2):222–35. [PubMed: 17918265]
- Dzhala VI, Staley KJ. Excitatory actions of endogenously released GABA contribute to initiation of ictal epileptiform activity in the developing hippocampus. *J Neurosci* 2003;23:1840–1846. [PubMed: 12629188]
- Dzhala VI, Talos DM, Sdrulla DA, Brumback AC, Mathews GC, Benke TA, Delpire E, Jensen FE, Staley KJ. NKCC1 transporter facilitates seizures in the developing brain. *Nat Med* 2005;11:1205–1213. [PubMed: 16227993]
- Ebihara S, Shirato K, Harata N, Akaike N. Gramicidin-perforated patch recording: GABA response in mammalian neurones with intact intracellular chloride. *J Physiol* 1995;484:77–86. [PubMed: 7541464]
- Fiumelli H, Cancedda L, Poo MM. Modulation of GABAergic transmission by activity via postsynaptic Ca²⁺-dependent regulation of KCC2 function. *Neuron* 2005;48:773–86. [PubMed: 16337915]
- Galanopoulou AS. Dissociated gender-specific effects of recurrent seizures on GABA signaling in CA1 pyramidal neurons: role of GABA(A) receptors. *J Neurosci* 2008;28:1557–1567. [PubMed: 18272677]
- Gale K. Subcortical structures and pathways involved in convulsive seizure generation. *J Clin Neurophysiol* 1992;9:264–77. [PubMed: 1350593]
- Ge S, Goh EL, Sailor KA, Kitabatake Y, Ming GL, Song H. GABA regulates synaptic integration of newly generated neurons in the adult brain. *Nature* 2006;439:589–93. [PubMed: 16341203]
- Gonzalez-Islas C, Chub N, Wenner P. NKCC1 and AE3 Appear to Accumulate Chloride in Embryonic Motoneurons. *J Neurophysiol* 2009;101:507–518. [PubMed: 19036864]
- Hammami S, Willumsen NJ, Olsen HL, Morera FJ, Latorre R, Klaerke DA. Cell volume and membrane stretch independently control K⁺ channel activity. *J Physiol* 2009;587:2225–2231. [PubMed: 19289549]
- Hannaert P, varez-Guerra M, Pirot D, Nazaret C, Garay RP. Rat NKCC2/NKCC1 cotransporter selectivity for loop diuretic drugs. *Naunyn Schmiedebergs Arch Pharmacol* 2002;365:193–199. [PubMed: 11882915]
- Holmes GL, Ben-Ari Y. The neurobiology and consequences of epilepsy in the developing brain. *Pediatr Res* 2001;49:320–325. [PubMed: 11228256]
- Hosford DA, Wang Y, Cao Z. Differential effects mediated by GABA_A receptors in thalamic nuclei in lh/lh model of absence seizures. *Epilepsy Res* 1997;27:55–65. [PubMed: 9169291]
- Huberfeld G, Wittner L, Clemenceau S, Baulac M, Kaila K, Miles R, Rivera C. Perturbed chloride homeostasis and GABAergic signaling in human temporal lobe epilepsy. *J Neurosci* 2007;27:9866–9873. [PubMed: 17855601]
- Hubner CA, Stein V, Hermans-Borgmeyer I, Meyer T, Ballanyi K, Jentsch TJ. Disruption of KCC2 reveals an essential role of K-Cl cotransport already in early synaptic inhibition. *Neuron* 2001;30:515–524. [PubMed: 11395011]
- Hughes JR. Absence seizures: a review of recent reports with new concepts. *Epilepsy Behav* 2009;15:404–12. [PubMed: 19632158]
- Huguenard JR, Alger BE. Whole-cell voltage-clamp study of the fading of GABA-activated currents in acutely dissociated hippocampal neurons. *J Neurophysiol* 1986;56:1–18. [PubMed: 3746390]
- Iadarola MJ, Gale K. Substantia nigra: site of anticonvulsant activity mediated by gamma-aminobutyric acid. *Science* 1982;218:1237–1240. [PubMed: 7146907]
- Ikedo M, Toyoda H, Yamada J, Okabe A, Sato K, Hotta Y, Fukuda A. Differential development of cation-chloride cotransporters and Cl⁻ homeostasis contributes to differential GABAergic actions between developing rat visual cortex and dorsal lateral geniculate nucleus. *Brain Res* 2003;984:149–159. [PubMed: 12932849]

- Kahle KT, Barnett SM, Sassower KC, Staley KJ. Decreased seizure activity in a human neonate treated with bumetanide, an inhibitor of the Na(+)-K(+)-2Cl(-) cotransporter NKCC1. *J Child Neurol* 2009;24:572–576. [PubMed: 19406757]
- Kahle KT, Staley KJ, Nahed BV, Gamba G, Hebert SC, Lifton RP, Mount DB. Roles of the cation-chloride cotransporters in neurological disease. *Nat Clin Pract Neurol* 2008;4:490–503. [PubMed: 18769373]
- Khalilov I, Holmes GL, Ben-Ari Y. In vitro formation of a secondary epileptogenic mirror focus by interhippocampal propagation of seizures. *Nat Neurosci* 2003;6:1079–1085. [PubMed: 14502289]
- Khosravani H, Pinnegar CR, Mitchell JR, Bardakjian BL, Federico P, Carlen PL. Increased high-frequency oscillations precede in vitro low-Mg seizures. *Epilepsia* 2005;46:1188–1197. [PubMed: 16060927]
- Kilb W, Sinning A, Luhmann HJ. Model-specific effects of bumetanide on epileptiform activity in the in-vitro intact hippocampus of the newborn mouse. *Neuropharmacology* 2007;53:524–533. [PubMed: 17681355]
- Kitayama M, Hirota K, Kudo M, Kudo T, Ishihara H, Matsuki A. Inhibitory effects of intravenous anaesthetic agents on K(+)-evoked glutamate release from rat cerebrocortical slices. Involvement of voltage-sensitive Ca(2+) channels and GABA(A) receptors Naunyn Schmiedebergs. *Arch Pharmacol* 2002;366:246–253.
- Krapf R, Berry CA, Verkman AS. Estimation of intracellular chloride activity in isolated perfused rabbit proximal convoluted tubules using a fluorescent indicator. *Biophys J* 1988;53:955–962. [PubMed: 3395662]
- Kreindler A, Zuckermann E, Steriade M, Chimion D. Electro-clinical features of convulsions induced by stimulation of brain stem. *J Neurophysiol* 1958;21:430–6. [PubMed: 13576185]
- Kuner T, Augustine GJ. A genetically encoded ratiometric indicator for chloride: capturing chloride transients in cultured hippocampal neurons. *Neuron* 2000;27:447–459. [PubMed: 11055428]
- Kyrozis A, Reichling DB. Perforated-patch recording with gramicidin avoids artifactual changes in intracellular chloride concentration. *J Neurosci Methods* 1995;57:27–35. [PubMed: 7540702]
- Li H, Tornberg J, Kaila K, Airaksinen MS, Rivera C. Patterns of cation-chloride cotransporter expression during embryonic rodent CNS development. *Eur J Neurosci* 2002;16:2358–2370. [PubMed: 12492431]
- Lopez-Samblas AM, Adams JA, Goldberg RN, Modi MW. The pharmacokinetics of bumetanide in the newborn infant. *Biol Neonate* 1997;72:265–272. [PubMed: 9395836]
- Macdonald RL, Twyman RE. Kinetic properties and regulation of GABAA receptor channels. *Ion Channels* 1992;3:315–343. [PubMed: 1384760]
- Mann EO, Paulsen O. Role of GABAergic inhibition in hippocampal network oscillations. *Trends Neurosci* 2007;30:343–349. [PubMed: 17532059]
- Marks DA, Katz A, Booke J, Spencer DD, Spencer SS. Comparison and correlation of surface and sphenoidal electrodes with simultaneous intracranial recording: an interictal study. *Electroencephalogr Clin Neurophysiol* 1992;82:23–29. [PubMed: 1370140]
- Misgeld U, Deisz RA, Dodt HU, Lux HD. The role of chloride transport in postsynaptic inhibition of hippocampal neurons. *Science* 1986;232:1413–1415. [PubMed: 2424084]
- Mizrahi EM, Kellaway P. Characterization and classification of neonatal seizures. *Neurology* 1987;37:1837–1844. [PubMed: 3683874]
- Murray DM, Boylan GB, Ali I, Ryan CA, Murphy BP, Connolly S. Defining the gap between electrographic seizure burden, clinical expression and staff recognition of neonatal seizures. *Arch Dis Child Fetal Neonatal Ed* 2008;93:F187–F191. [PubMed: 17626147]
- Oddo M, Carrera E, Claassen J, Mayer SA, Hirsch LJ. Continuous electroencephalography in the medical intensive care unit. *Crit Care Med* 2009;37:2051–2056. [PubMed: 19384197]
- Owens DF, Boyce LH, Davis MB, Kriegstein AR. Excitatory GABA responses in embryonic and neonatal cortical slices demonstrated by gramicidin perforated-patch recordings and calcium imaging. *J Neurosci* 1996;16:6414–6423. [PubMed: 8815920]
- Painter MJ, Scher MS, Stein AD, Armatti S, Wang Z, Gardiner JC, Paneth N, Minnigh B, Alvin J. Phenobarbital compared with phenytoin for the treatment of neonatal seizures. *N Engl J Med* 1999;341:485–489. [PubMed: 10441604]

- Palma E, Amici M, Sobrero F, Spinelli G, Di AS, Ragozzino D, Mascia A, Scopetta C, Esposito V, Mileli R, Eusebi F. Anomalous levels of Cl⁻ transporters in the hippocampal subiculum from temporal lobe epilepsy patients make GABA excitatory. *Proc Natl Acad Sci U S A* 2006;103:8465–8468. [PubMed: 16709666]
- Payne JA, Rivera C, Voipio J, Kaila K. Cation-chloride co-transporters in neuronal communication, development and trauma. *Trends Neurosci* 2003;26:199–206. [PubMed: 12689771]
- Plotkin MD, Snyder EY, Hebert SC, Delpire E. Expression of the Na-K-2Cl cotransporter is developmentally regulated in postnatal rat brains: a possible mechanism underlying GABA's excitatory role in immature brain. *J Neurobiol* 1997;33:781–795. [PubMed: 9369151]
- Quilichini PP, Diabira D, Chiron C, Milh M, Ben-Ari Y, Gozlan H. Effects of antiepileptic drugs on refractory seizures in the intact immature corticohippocampal formation in vitro. *Epilepsia* 2003;44:1365–1374. [PubMed: 14636342]
- Rennie JM. Neonatal seizures. *Eur J Pediatr* 1997;156:83–87. [PubMed: 9039506]
- Rennie JM, Boylan GB. Neonatal seizures and their treatment. *Curr Opin Neurol* 2003;16:177–181. [PubMed: 12644746]
- Rheims S, Holmgren CD, Chazal G, Mulder J, Harkany T, Zilberter T, Zilberter Y. GABA Action in Immature Neocortical Neurons Directly Depends on the Availability of Ketone Bodies. *J Neurochem* 2009;110:1330–1338. [PubMed: 19558450]
- Rheims S, Minlebaev M, Ivanov A, Represa A, Khazipov R, Holmes GL, Ben-Ari Y, Zilberter Y. Excitatory GABA in Rodent Developing Neocortex In Vitro. *J Neurophysiol* 2008a;100:609–619. [PubMed: 18497364]
- Rheims S, Represa A, Ben-Ari Y, Zilberter Y. Layer-specific generation and propagation of seizures in slices of developing neocortex: role of excitatory GABAergic synapses. *J Neurophysiol* 2008b;100:620–628. [PubMed: 18497363]
- Rivera C, Voipio J, Payne JA, Ruusuvuori E, Lahtinen H, Lamsa K, Pirvola U, Saarna M, Kaila K. The K⁺/Cl⁻ co-transporter KCC2 renders GABA hyperpolarizing during neuronal maturation. *Nature* 1999;397:251–255. [PubMed: 9930699]
- Romero MF, Fulton CM, Boron WF. The SLC4 family of HCO₃⁻ transporters. *Pflugers Arch* 2004;447:495–509. [PubMed: 14722772]
- Roos A, Boron WF. Intracellular pH. *Physiol Rev* 1981;61:296–434. [PubMed: 7012859]
- Scher MS, Alvin J, Gaus L, Minnigh B, Painter MJ. Uncoupling of EEG-clinical neonatal seizures after antiepileptic drug use. *Pediatr Neurol* 2003;28:277–280. [PubMed: 12849880]
- Shimizu-Okabe C, Yokokura M, Okabe A, Ikeda M, Sato K, Kilb W, Luhmann HJ, Fukuda A. Layer-specific expression of Cl⁻ transporters and differential [Cl⁻]_i in newborn rat cortex. *Neuroreport* 2002;13:2433–2437. [PubMed: 12499844]
- Sipila ST, Schuchmann S, Voipio J, Yamada J, Kaila K. The cation-chloride cotransporter NKCC1 promotes sharp waves in the neonatal rat hippocampus. *J Physiol* 2006;573:765–773. [PubMed: 16644806]
- Staley K. The role of an inwardly rectifying chloride conductance in postsynaptic inhibition. *J Neurophysiol* 1994;72:273–284. [PubMed: 7965011]
- Staley K, Smith R, Schaack J, Wilcox C, Jentsch TJ. Alteration of GABA_A receptor function following gene transfer of the CLC-2 chloride channel. *Neuron* 1996;17:543–551. [PubMed: 8816717]
- Staley KJ, Proctor WR. Modulation of mammalian dendritic GABA(A) receptor function by the kinetics of Cl⁻ and. *J Physiol* 1999;519(Pt 3):693–712. [PubMed: 10457084]
- Stein V, Hermans-Borgmeyer I, Jentsch TJ, Hubner CA. Expression of the KCl cotransporter KCC2 parallels neuronal maturation and the emergence of low intracellular chloride. *J Comp Neurol* 2004;468:57–64. [PubMed: 14648690]
- Sullivan JE, Witte MK, Yamashita TS, Myers CM, Blumer JL. Pharmacokinetics of bumetanide in critically ill infants. *Clin Pharmacol Ther* 1996;60:405–413. [PubMed: 8873688]
- Sung KW, Kirby M, McDonald MP, Lovinger DM, Delpire E. Abnormal GABA_A receptor-mediated currents in dorsal root ganglion neurons isolated from Na-K-2Cl cotransporter null mice. *J Neurosci* 2000;20:7531–7538. [PubMed: 11027211]

- Tekgul H, Gauvreau K, Soul J, Murphy L, Robertson R, Stewart J, Volpe J, Bourgeois B, du Plessis AJ. The current etiologic profile and neurodevelopmental outcome of seizures in term newborn infants. *Pediatrics* 2006;117:1270–80. [PubMed: 16585324]
- Thompson SM, Gahwiler BH. Activity-dependent disinhibition. I Repetitive stimulation reduces IPSP driving force and conductance in the hippocampus in vitro. *J Neurophysiol* 1989;61:501–511. [PubMed: 2709096]
- Twyman RE, Rogers CJ, Macdonald RL. Differential regulation of gamma-aminobutyric acid receptor channels by diazepam and phenobarbital. *Ann Neurol* 1989;25:213–2. [PubMed: 2471436]
- Tyzio R, Holmes GL, Ben-Ari Y, Khazipov R. Timing of the developmental switch in GABA(A) mediated signaling from excitation to inhibition in CA3 rat hippocampus using gramicidin perforated patch and extracellular recordings. *Epilepsia* 2007;48(Suppl 5):96–105. [PubMed: 17910587]
- Tyzio R, Ivanov A, Bernard C, Holmes GL, Ben-Ari Y, Khazipov R. Membrane potential of CA3 hippocampal pyramidal cells during postnatal development. *J Neurophysiol* 2003;90:2964–2972. [PubMed: 12867526]
- Wang C, Shimizu-Okabe C, Watanabe K, Okabe A, Matsuzaki H, Ogawa T, Mori N, Fukuda A, Sato K. Developmental changes in KCC1, KCC2, and NKCC1 mRNA expressions in the rat brain. *Brain Res Dev Brain Res* 2002;139:59–66.
- Wang DD, Kriegstein AR. GABA regulates excitatory synapse formation in the neocortex via NMDA receptor activation. *J Neurosci* 2008;28:5547–5558. [PubMed: 18495889]
- Weiner SP, Painter MJ, Geva D, Guthrie RD, Scher MS. Neonatal seizures: electroclinical dissociation. *Pediatr Neurol* 1991;7:363–368. [PubMed: 1764139]
- Wells JE, Porter JT, Agmon A. GABAergic inhibition suppresses paroxysmal network activity in the neonatal rodent hippocampus and neocortex. *J Neurosci* 2000;20:8822–8830. [PubMed: 11102490]
- White LE, Price JL. The functional anatomy of limbic status epilepticus in the rat. I Patterns of 14C-2-deoxyglucose uptake and Fos immunocytochemistry. *J Neurosci* 1993;13:4787–4809. [PubMed: 8229199]
- Yamada J, Okabe A, Toyoda H, Kilb W, Luhmann HJ, Fukuda A. Cl⁻ uptake promoting depolarizing GABA actions in immature rat neocortical neurones is mediated by NKCC1. *J Physiol* 2004;557:829–841. [PubMed: 15090604]
- Yan Y, Dempsey RJ, Flemmer A, Forbush B, Sun D. Inhibition of Na⁽⁺⁾-K⁽⁺⁾-Cl⁽⁻⁾ cotransporter during focal cerebral ischemia decreases edema and neuronal damage. *Brain Res* 2003;961:22–31. [PubMed: 12535773]
- Zar, JH. *Biostatistical Analysis*. Upper Saddle River: Prentice Hall; 1999. Comparing Simple Linear Regression equations; p. 360-376.
- Zhang YF, Coulter DA. Anticonvulsant drug effects on spontaneous thalamocortical rhythms in vitro: phenytoin, carbamazepine, and phenobarbital. *Epilepsy Res* 1996;23:55–70. [PubMed: 8925803]
- Zhang YF, Gibbs JW III, Coulter DA. Anticonvulsant drug effects on spontaneous thalamocortical rhythms in vitro: ethosuximide, trimethadione, and dimethadione. *Epilepsy Res* 1996;23:15–36. [PubMed: 8925801]
- Zhu L, Lovinger D, Delpire E. Cortical neurons lacking KCC2 expression show impaired regulation of intracellular chloride. *J Neurophysiol* 2005;93:1557–1568. [PubMed: 15469961]

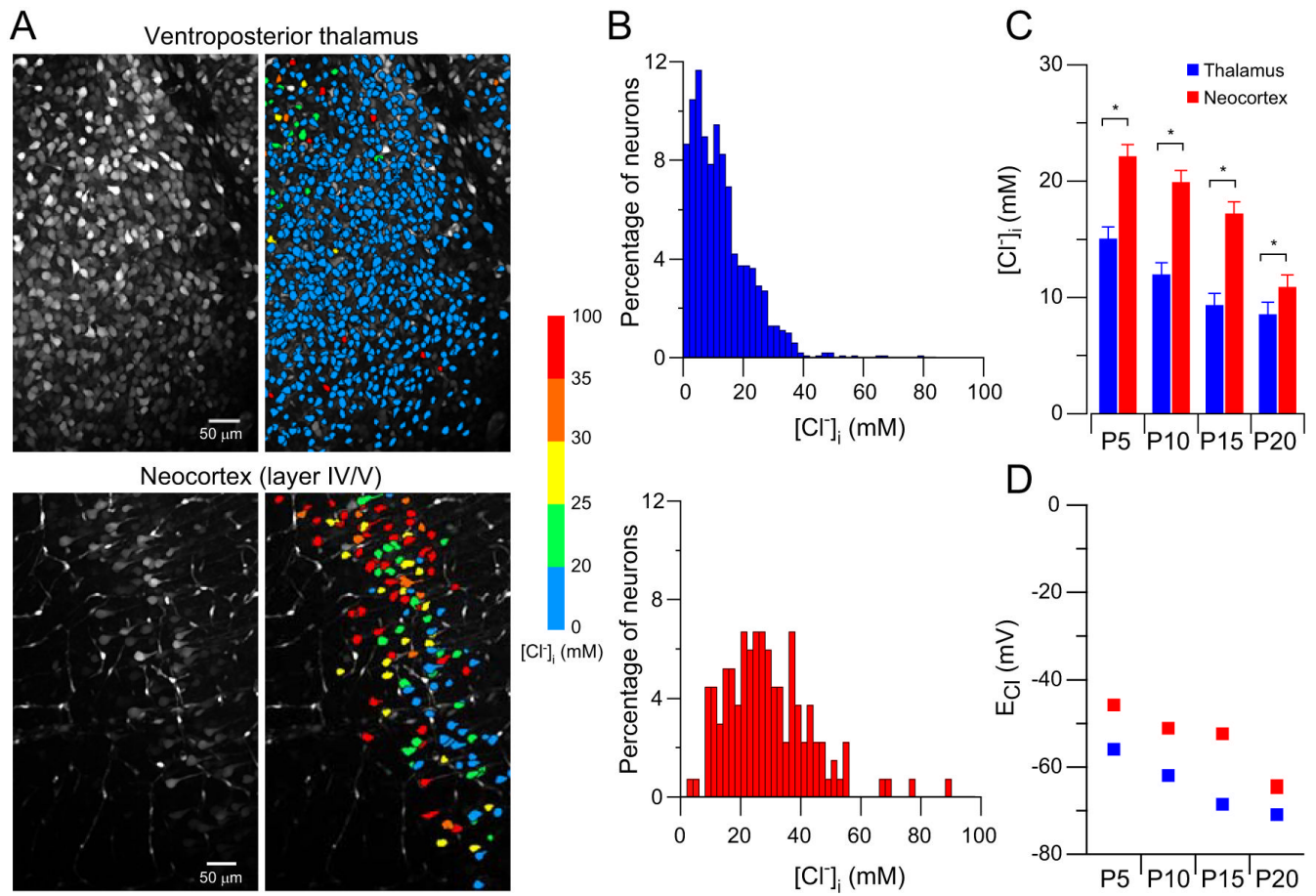


Figure 1. Thalamus has lower $[Cl^-]_i$ than the neocortex in early post-natal development
 A) Two-photon imaging of Clomeleon in the ventroposterior thalamus and neocortex (layer IV/V) at P10; overlay of multiple planes. *Left panel*: YFP fluorescence. *Right panel*: neuronal somata pseudo-colored to a single value according to $[Cl^-]_i$ averaged over the soma. B) Histogram of $[Cl^-]_i$ from the neurons depicted in A. C) Differences in $[Cl^-]_i$ between thalamus and neocortex during development (* indicates statistical significance, Table 1; $n=15$ mice). D) E_{Cl} calculated using the Nernst equation at 33 °C for each slice. Mean \pm SEM

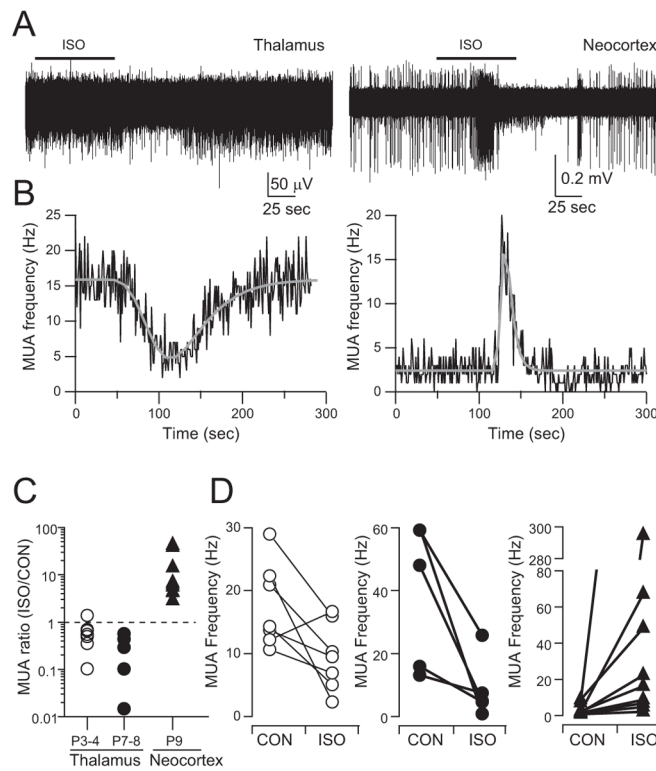


Figure 2. The thalamus is inhibited while the neocortex is depolarized during early development
 A) MUA recordings from ventroposterior thalamus (left, P7) and neocortex (right, P9) in the presence of 2 mM kynurenic acid. High-pass filtered at 50 Hz. B) MUA frequency plotted from the same traces indicated above; peak function fit indicated by red line. C) Isoguvacine to control ratio (ISO/CON) of MUA frequency in the thalamus (\bullet) and neocortex (\blacktriangle) at P3-4 (blank) and P7-8 (filled). D) Individual thalamus and neocortex responses to 10 μ M isoguvacine at P3-4, P7-8 and P9.

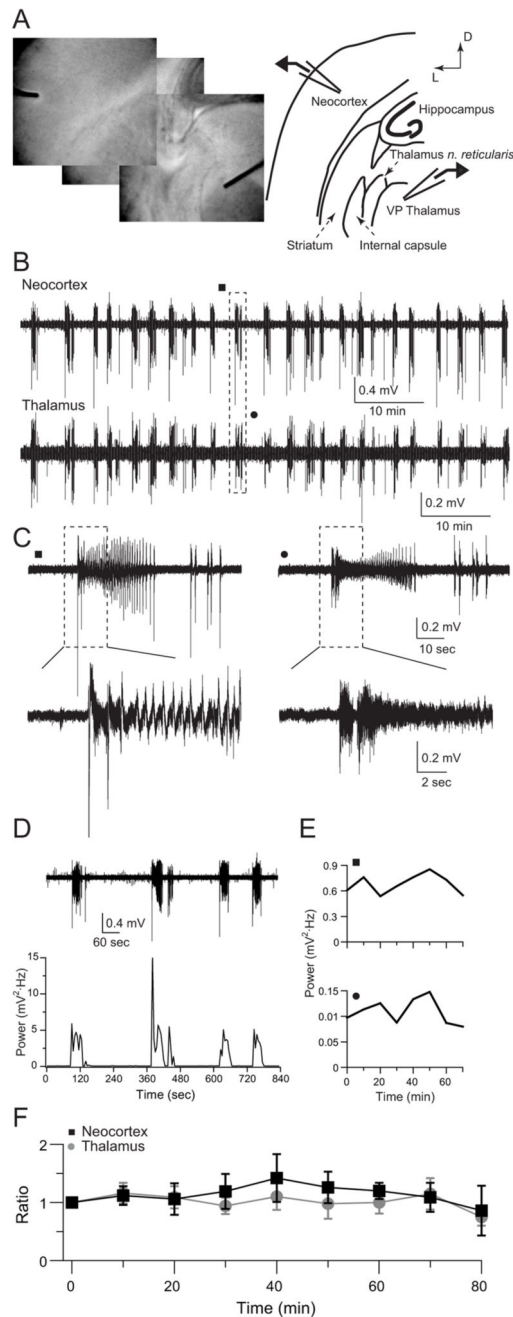


Figure 3. Spontaneous thalamo-cortical epileptiform activity during early development is stable over time

A) *Left panel*: Combined thalamo-cortical slice imaged in the recording chamber. *Right panel*: Schematic representation of the thalamo-cortical slice and the typical position of the recording electrodes (D: dorsal, L: lateral). B) Simultaneous extracellular recording from neocortex layer IV/V (top, ■) and ventroposterior thalamus (bottom, ●) in low-Mg²⁺ (P9). C) Higher magnifications of ictal events depicted in dashed boxes in A. D) *Top*: First 4 neocortical ictal events from A; *bottom*: Signal power calculated every 5 sec, showing increase power during epileptiform events. E) Entire trace signal power calculated every 10 min from neocortex (top) and thalamus (bottom). EEG band (1–160Hz). F) Ratio of each 10 min to the

first 10 min during an 80 min recording. No statistical differences between each 10 min segment (NEO: $F(8,35)=0.20$, $p=0.99$; THA: $F(8,35)=0.55$, $p=0.81$; $n=5$ slices; One-way ANOVA).

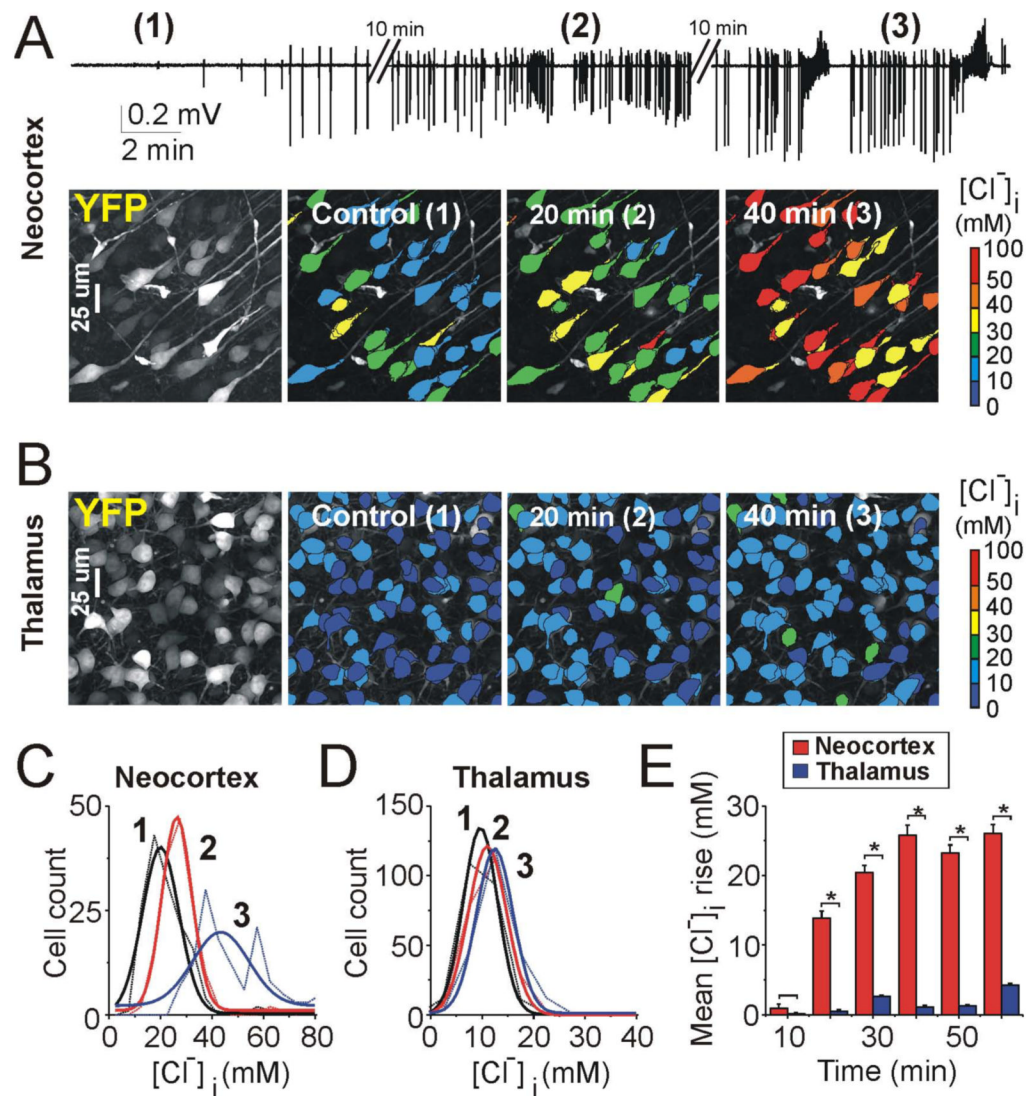


Figure 4. Effects of epileptiform activity on $[Cl^-]_i$ in the thalamo-cortical slices

A) Extracellular field potential recording in neocortex layer IV/V in the thalamo-cortical slice preparation from P10 CLM-1 mouse. Epileptiform discharges were induced by low- Mg^{2+} ACSF. Examples of two-photon confocal imaging of YFP (*left*) in neocortical neurons pseudo-colored to represent $[Cl^-]_i$ in control (1), 20 min (2) and 40 min (3) after onset of epileptiform discharges. B) Examples of two-photon imaging of YFP (*left*) in neurons in the ventro-posterior thalamus, pseudo-colored to represent $[Cl^-]_i$ in control (1), 20 min (2) and 40 min (3) after onset of epileptiform discharges. Epileptiform discharges were induced and recorded as assayed in part A. C–D) Corresponding changes of $[Cl^-]_i$ in control and during epileptiform activity. Distribution of $[Cl^-]_i$ (bin size 5 mM) in neocortex (C; 150 neurons) and thalamus (D; 227 neurons) in control (1), 20 min (2) and 40 min (3) after onset of epileptiform discharges. Gauss fits yielded corresponding means and standard deviations of 20 ± 0.6 mM (1), 26.3 ± 0.2 mM (2) and 43.4 ± 2.3 mM (3) in the neocortex (C) and 10 ± 0.2 mM (1), 11.1 ± 0.2 mM (2) and 13.2 ± 0.3 mM (3) in the thalamus. E) Summary effects of epileptiform activity on intracellular chloride accumulation (mean \pm s.e.; *indicates statistical significance) in the neocortex (268 neurons from $n = 3$ slices at P9–10) and thalamus (348 neurons from $n = 2$ slices at P9–10).

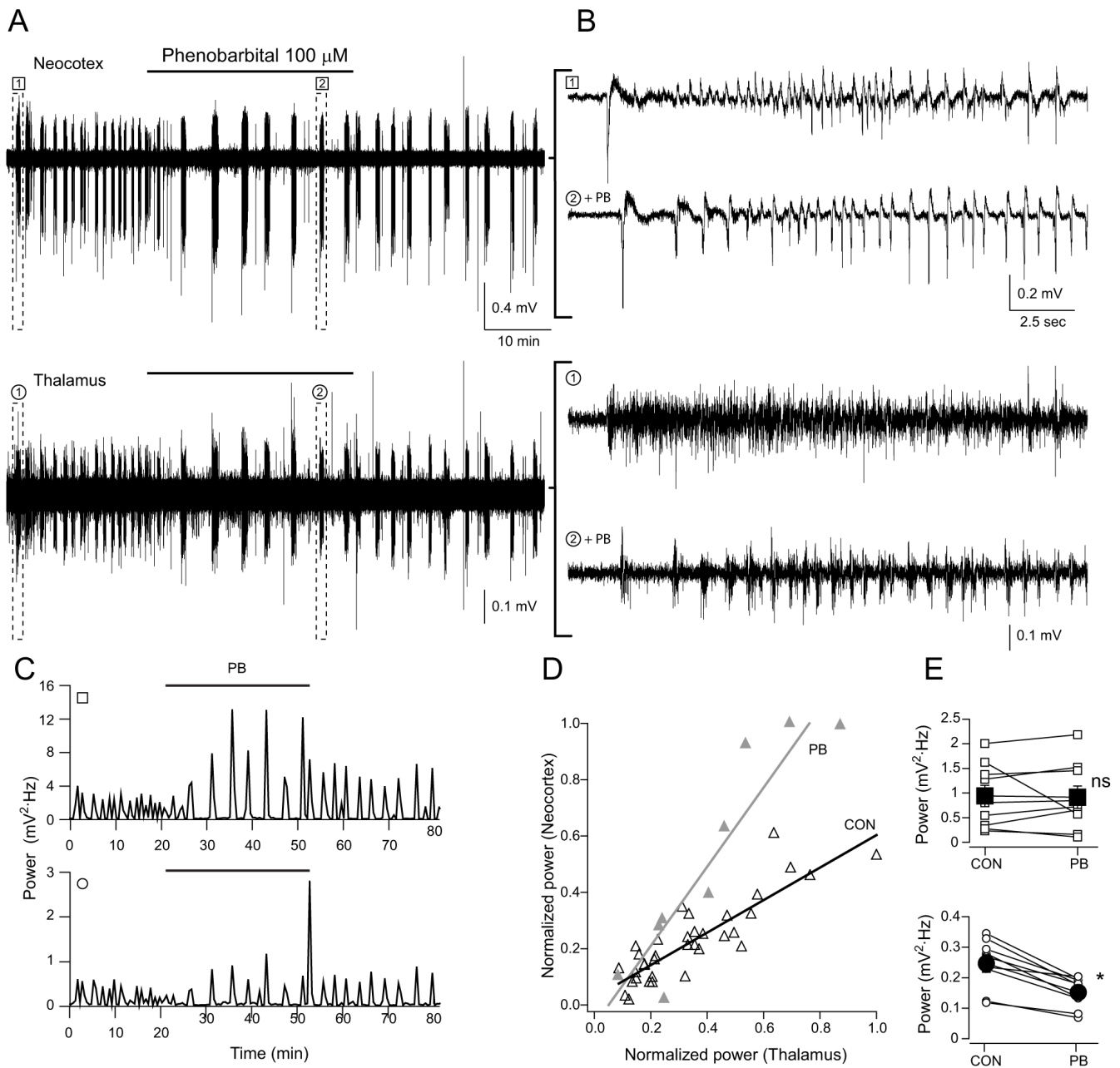


Figure 5. Phenobarbital reduces the power of epileptiform activity in thalamus but not in the neocortex

A) Simultaneous extracellular recording from a thalamo-cortical slice in low- Mg^{2+} (P9). Dashed boxes indicated higher magnification segments in B (□ neocortex, ○ thalamus). B) Higher magnification of the initial segment of two ictal events: (1) control and (2) during 100 μ M phenobarbital. C) Signal power (EEG band) determined every 30 seconds during the recording depicted in A. D) Linear correlation of the ictal signal power between thalamus and neocortex. Power was normalized to the maximum ictal event obtained from C. Control (Δ), phenobarbital (\blacktriangle). Line represents linear regression (CON[black]: $r=0.87\pm0.09$, $p<0.001$; $n=35$. PB[gray] $r=0.92\pm0.15$, $p<0.001$, $n=9$). The linear regression slopes are statistically

different (CON: 0.58; PB: 1.40; $p < 0.001$). E) Effect of phenobarbital on individual recordings (* indicates $p < 0.001$; ns indicates $p = 0.838$). Filled symbol indicates mean \pm SEM.

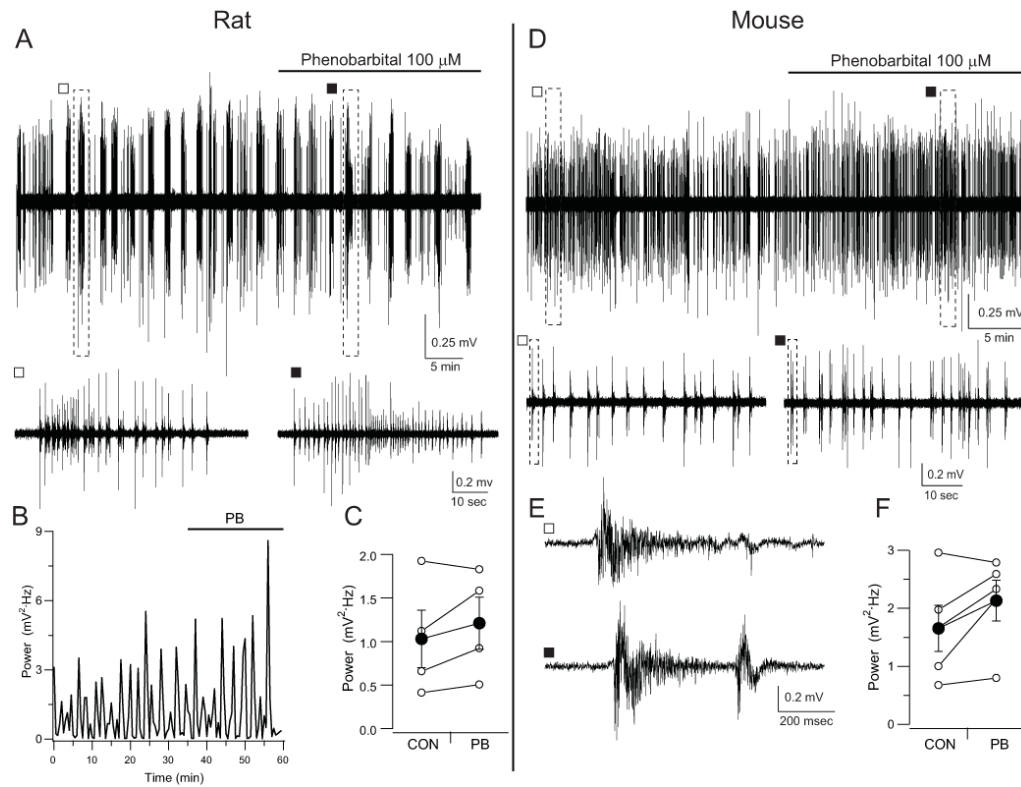


Figure 6. Phenobarbital is ineffective in the electrically disconnected neocortex

A) Extracellular recording of spontaneous epileptiform activity from the rat neocortex (P8) in low- Mg^{2+} . Dashed boxes indicate higher magnification segments during control (\square) and 100 μM phenobarbital (\blacksquare) in the lower panels. B) Signal power (EEG band) determined every 30 seconds during the recording depicted in A. C) Effect of phenobarbital on individual recordings, filled symbol indicates mean \pm SEM ($p=0.224$, paired t -test). D) Same as A but recorded in a P11 Clomeleon mice. E) Higher magnification of events depicted in the middle panel (control \square ; phenobarbital \blacksquare). F) Effect of phenobarbital on individual recordings, filled symbol indicates mean \pm SEM ($p=0.106$, paired t -test).

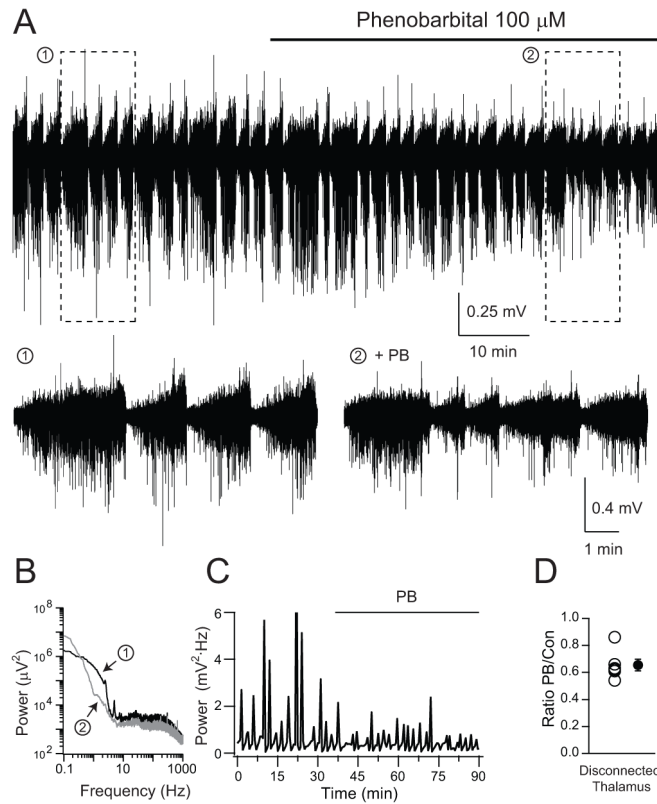


Figure 7. Phenobarbital decreases epileptiform activity in the disconnected thalamus

A) Extracellular recording of spontaneous epileptiform activity from the electrically disconnected rat thalamus (P10) in low-Mg²⁺ plus 100 μM 4-AP. Dashed boxes indicate higher magnification segments during control (1) and 100 μM phenobarbital (2) in the lower panels. B) Fast Fourier Transform of the segments depicted in the lower panels of A. C) Signal power (EEG band) determined every 30 seconds during the recording depicted in A. D) Phenobarbital to control ratio of all slices recorded. Filled symbol indicates mean±SEM ($n=6$; $p<0.001$, one sample t -test).

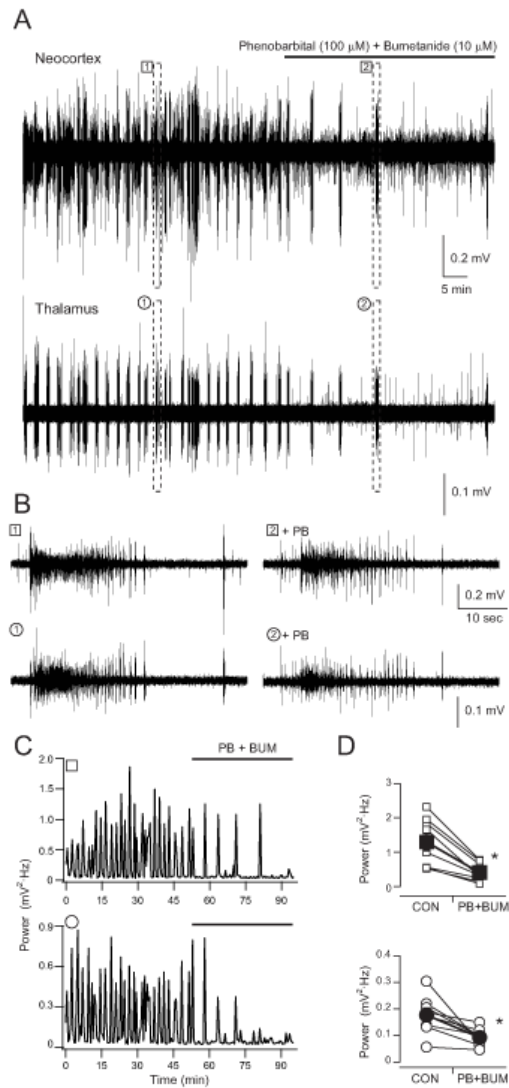


Figure 8. Co-application of phenobarbital and bumetanide decreases the epileptiform activity in the neocortex

A) Simultaneous extracellular recording from a thalamo-cortical slice in low- Mg^{2+} (P10). Dashed boxes indicated higher magnification segments in B (\square neocortex, \circ thalamus). B) Higher magnification of two ictal events: (1) control and (2) during 100 μM phenobarbital and 10 μM bumetanide. C) Signal power (EEG band) determined every 30 seconds during the recording depicted in A. Line indicates the presence of 100 μM phenobarbital and 10 μM bumetanide. D) Effect of phenobarbital on individual recordings (*, indicates $p=0.010$ for neocortex; $p=0.011$ for thalamus; paired t -test). Filled symbol indicates mean \pm SEM.

Table 1
[Cl⁻]_i differences between ventroposterior thalamus and neocortex (layer IV/V)

[Cl⁻]_i measurements obtained from Clomeleon expressing neurons at the corresponding age. *n* represents the number of cells. *P* values correspond to Wilcoxon-Mann-Whitney test.

	Thalamus		Neocortex		<i>P</i>
	[Cl ⁻] _i	<i>n</i>	[Cl ⁻] _i	<i>n</i>	
P5-6	15.1±1.01	8,950	22.1±1.03	968	<0.001
P10-11	12.0±1.01	5,923	18.1±1.02	1,734	<0.001
P15-16	9.3±1.02	5,645	17.2±1.02	2,389	<0.001
P20	8.5±1.04	741	10.9±1.06	411	<0.001